Original Article

Strategy for improving cell-mediated vascularized soft tissue formation in a hydrogen peroxide-triggered chemically-crosslinked hydrogel

Journal of Tissue Engineering
Volume 13: 1–20

DOI: 10.1177/20417314221084096
journals.sagepub.com/home/tej
SAGE

Shih-Yen Wei, Tzu-Hsuan Chen, Feng-Sheng Kao, Yi-Jung Hsu and Ying-Chieh Chen

Abstract

The physically-crosslinked collagen hydrogels can provide suitable microenvironments for cell-based functional vascular network formation due to their biodegradability, biocompatibility, and good diffusion properties. However, encapsulation of cells into collagen hydrogels results in extensive contraction and rapid degradation of hydrogels, an effect known from their utilization as a pre-vascularized graft in vivo. Various types of chemically-crosslinked collagen-based hydrogels have been successfully synthesized to decrease volume contraction, retard the degradation rate, and increase mechanical tunability. However, these hydrogels failed to form vascularized tissues with uniformly distributed microvessels in vivo. Here, the enzymatically chemically-crosslinked collagen-Phenolic hydrogel was used as a model to determine and overcome the difficulties in engineering vascular networks. Results showed that a longer duration of inflammation and excessive levels of hydrogen peroxide limited the capability for blood vessel forming cells-mediated vasculature formation in vivo. Lowering the unreacted amount of crosslinkers reduced the densities of infiltrating host myeloid cells by half on days 2–4 after implantation, but blood vessels remained at low density and were mainly located on the edge of the implanted constructs. Co-implantation of a designed spacer with cell-laden hydrogel maintained the structural integrity of the hydrogel and increased the degree of hypoxia in embedded cells. These effects resulted in a two-fold increase in the density of perfused blood vessels in the hydrogel. Results agreed with computer-based simulations. Collectively, our findings suggest that simultaneous reduction of the crosslinker-induced host immune response and increase in hypoxia in hydrogen peroxide-triggered chemically-crosslinked hydrogels can effectively improve the formation of cell-mediated functional vascular networks.

Keywords

Vascular tissue engineering, enzymatically crosslinked, phenolic-protein hydrogels, collagen contraction

Date received: 22 August 2021; accepted: 13 February 2022

Introduction

Collagen with arginine-glycine-aspartic acid (RGD) and matrix metallo-proteinase (MMP) sequences that cells can attach to and degrade, respectively, is extensively used in bone repair and vascular tissue engineering.[1–4] However, its mechanical instability, rapid degradation, and volume shrinkage[5] limit its application to large areas of tissue injury. Research studies have attempted to form physically-crosslinked collagen hydrogels to reduce the volume shrinkage rate by increasing the concentration of collagen prepolymer solutions or adding fibrin into collagen hydrogels.[6–9] Nonetheless, such hydrogels suffer from rapid biodegradability and poor mechanical strength; additionally,

Department of Materials Science and Engineering, National Tsing Hua University, Hsinchu, Taiwan

Corresponding author:
Ying-Chieh Chen, Department of Materials Science and Engineering, National Tsing Hua University, 101, Section 2, Kuang-Fu Road, Hsinchu 30013, Taiwan.
Email: yisschen@mx.nthu.edu.tw

higher collagen concentrations and increased stiffness negatively affected cell bioactivity and microvessel formation. Other studies synthesized injectable chemically-crosslinked collagen hydrogels formed by conjugating functional groups on collagen molecules. This approach led to improvements in thermal stability, retention volume, and mechanical properties,[10–13] but the presence of crosslinking agents significantly decreased the bioactivity of the cells encapsulated into the hydrogel.[14–16] Endothelial colony-forming cells (ECFCs) formed mature microvessels covered by pericytes in chemically-crosslinked collagen gels at a subcutaneous site in mice within 1 week, but most ECFC-lined vessels were located at the edge region of explants.[7,16] The usefulness of chemically-crosslinked collagen hydrogels as supportive material for cell-mediated vascular network formation remains limited.

Phenolic (Ph)-protein hydrogels with independently tunable gelation time and stiffness have been used as carriers in drug delivery[17,18] and tissue engineering.[7,19,20] Besides collagen-Ph hydrogels, Ph groups were also conjugated on hyaluronic acid (HA) and gelatin to form HA-Ph and gelatin-Ph hydrogels, respectively. Most previous studies used HA-Ph hydrogels to modulate the differentiation of stem cells to chondrocytes, hepatocytes, or neural lineages. It was confirmed that HA-Ph hydrogels can stimulate stem cell differentiation and matrix synthesis in vitro.[19–22] In the absence of cytokines, HA-Ph hydrogels have limited capability for cartilage repair in vivo.[23–25] The gelatin-Ph hydrogel is biocompatible and biodegradable in vivo and causes neither necrosis of surrounding tissues nor server-host immune responses.[26–28] Two-dimensional co-culture of human umbilical vein endothelial cells (HUVECs) and human dermal fibroblasts on three-dimensional printed gelatin-Ph hydrogels showed cell spreading on the hydrogels in vitro.[29] Some groups conjugated vascular endothelial growth factor (VEGF)[30] or co-encapsulated ECFCs and mesenchymal stem cells (MSCs)[31] into gelatin-Ph hydrogels, which were subcutaneously injected into a mouse to form the cell-laden implants. After 7 days, perfused human microvessels were only observed in the edge region of the implanted hydrogel. Numerous studies have used Ph-crosslinked protein-based hydrogels with added growth factors and cytokines to improve bone/cartilage repair and vascular tissue engineering.[23–25,30,31] In our previous studies, in the absence of growth factors and cytokines in gelatin-Ph or collagen-Ph hydrogels, engineered microvessels were mainly located at the edge region of explants, implying the presence of factors that interfere with cell-mediated vascular network formation in Ph-crosslinked hydrogels.[16,31] The cell response to chemically-crosslinked collagen hydrogels in vitro and in vivo is a critical challenge that must be to improve their capability of tissue regeneration. In this study, collagen-Ph hydrogels were synthesized and used as a representative model material to culture and deliver cells in vitro and in vivo; physically-crosslinked collagen hydrogels served as the control. Optimization of the vascularization strategy may provide valuable knowledge for constructing vascularized tissues in hydrogen peroxide (H_2O_2)-triggered chemically-crosslinked hydrogels.

Experimental section

Preparation and characterization of collagen and collagen-phenolic hydroxyl conjugates (collagen-Ph conjugate)

To extract collagen, rabbit skin tissues were cut into small pieces (~1 cm^2) and soaked in 95% (w/v) ethanol for 2 min to remove debris and sterilize skin tissues. Then, immersing it in 0.1 M sodium hydroxide at 4°C for 24 h, rinsing with deionized water three times, and reacting with 10% (w/v) butanol at 4°C for additional 24 h to remove fat from skin tissues. After rinsing with deionized water three times, collagen was extracted from skin tissues at a ratio of skin: 0.5 M acetic acid = 1 g: 9 mL at 4°C, and the resulting solution was collected every day in four consecutive days. Lastly, the extracted solution was centrifuged at 11,700 g for 10 min at 4°C to remove impurities, salted out by adding sodium chloride to a final concentration of 3 M, and centrifuged again to separate the precipitate from the solution. The precipitate was collected and redissolved in 0.5 M acetic acid for 1 day, dialyzed against deionized water, and finally lyophilized in a freeze-dryer to have lyophilized collagen. The preparation processes of collagen were performed under sterile conditions.

To synthesize collagen-Ph conjugates, freeze-dried collagen was dissolved into 40 mL of 0.0625% (w/v) hydrogen chloride aqueous solution with 0.78 g of 2-(N-Morpholino) ethane sulfonic acid hydrate (MES, Sigma-Aldrich, USA) as a pH buffer, and adjusted the pH value to 6 by adding 4 M sodium hydroxide aqueous solution. After completely dissolving, 0.135 g of N-(3-Dimethylaminopropyl)-N′-ethylcarbodiimide hydrochloride (EDC, Sigma-Aldrich, USA), 0.032 g of N-Hydroxysuccinimide (NHS, Sigma-Aldrich, USA), and 0.168 g of tyramine hydrochloride (Sigma-Aldrich, USA) were added and reacted at 4°C for 24 h under the continuous stirring condition. When the reaction was terminated, the solutions were dialyzed against 0.004 M hydrogen chloride aqueous solution using a 3.5 K MWCO dialysis bag until the absorption peak caused by the residual tyramine at 275 nm could not be detected by UV/Visible spectroscopy (Amersham Biosciences, USA) and finally lyophilized in a freeze-dryer to have lyophilized collagen-Ph conjugates. The preparation processes of collagen-Ph were performed under sterile conditions.

Preparation and characterization of collagen and collagen-Ph hydrogels

At 4°C, the freeze-dried collagen was completely dissolved in 0.02 M acetic acid at 0.15%, 0.3%, and 0.6% (w/v). Before use, 1 mL of collagen prepolymer solution was

prepared by 0.9 mL of 0.15%, 0.3%, or 0.6% (w/v) collagen solution, 0.1 mL calcium and magnesium-free phosphate-buffered saline (DPBS), 0.025 mL 4-(2-hydroxyethyl)-1-piperazineethanesulfonic acid (HEPES) at pH 7 by adding suitable amounts of 1 M sodium hydroxide on ice. Then, the collagen prepolymer solutions were delivered into a culture dish to allow its self-assembly gelation at 37°C to form the collagen hydrogel (Collagen). The endotoxin testing (Thermo Scientific Cat # 88282, USA) was performed to determine the quantification of endotoxin in collagen-based hydrogels. After considering the dilution factor, the final endotoxin concentration was determined to be 0.26 EU/mL for collagen and 0.42 EU/ml for collagen-Ph, which are lower than the Food and Drug Administration guidance ($<$ 0.5 EU/mL) for industry pyrogen and endotoxins testing. The freeze-dried collagen-Ph conjugates were completely dissolved in PBS at 0.7% (w/v). Then, the collagen-Ph aqueous solution is thoroughly mixed with 78 units/mL of horseradish peroxidase (HRP) and 28.5 μM of hydrogen peroxide (H_2O_2) to form chemically crosslinked Collagen-Ph hydrogel at 37°C.

Using circular dichroism (CD) measurements, all samples were adjusted to 0.3% (w/v). The solution was scanned at the wavelength range of 190–260 nm at 4°C, and molar ellipticity was recorded using a CD apparatus (AVIV Biomedical Inc. CD4100).

For characterizing the degrees of functional group substitution on collagen-Ph conjugates, lyophilized collagen, and collagen-Ph powder was dissolved in heavy water (D_2O) at 0.2% (w/v) and measured the chemical shift with a high-magnetic-field proton nuclear magnetic resonance (^{1}H-NMR) instrument (AVANCE-500, Bruker, USA).

An atomic force microscope (Dimension FastScan AFM, Bruker, USA) was used to study collagen fibril formation of the Collagen and Collagen-Ph hydrogels. Each prepolymer solution was prepared and dropped on the mica substrates and imaged by square pyramidal silicon nitride tips of spring constant 0.09 N/m (Olympus BL-AC40TS) every 15 min until gelation finished.

For the mechanical properties test, the mechanical strength of each hydrogel was measured in a strain-controlled rheometer (AR-G2, TA instruments, USA) with parallel plate (25 mm diameter plates) in the oscillatory mode at room temperature. The storage modulus (G′) was acquired as the strain amplitudes from 0.01% to 500% with an angular frequency of 10 rad/s.

The microstructures of the hydrogels were characterized by confocal microscopy and scanning electron microscopy (SEM). To visualize the microstructures of the hydrogel in an aqueous environment, a fluorescent dye, Atto 425 NHS ester (Sigma-Aldrich, USA), was used to label the amine side groups according to manufacturer's instructions and imaged under a confocal microscope (TCS-SP5-X AOBS, Leica, Germany). To further study the microstructure of hydrogels in a lyophilized state, we placed the swollen hydrogel at −80°C for 24 h and then placed it in a freeze-dryer for 1 days. Then, the microstructures of the freeze-dried hydrogels were obtained by using scanning electron microscopy (SEM) (S-4300, Hitachi, Japan).

To study the adsorption profiles of hydrogel, the crosslinked hydrogels were immersed in 2 mg/mL fluorescein isothiocyanate-dextran (70 kDa FITC-dextran, Sigma-Aldrich) solutions at 2, 4, 6, 8, 12, and 24 h. Then, the hydrogels were washed three times with PBS and soaked in fresh PBS to measure the absorption profile of the FITC-dextran by measuring the FITC intensity with a UV-visible spectrophotometer (SpectraMax Plus 384, Molecular Devices, USA) at an excitation wavelength of 495 nm. To study the releasing profiles of hydrogel, after 24 h of absorption, the hydrogels were washed three times with PBS and soaked in PBS to measure their cumulative release profiles for FITC-dextran at 2, 4, 6, 8, 12, and 24 h according to prior protocol.

Cell culture

Human umbilical vein endothelial cells (HUVECs, Lonza, USA) cultured in endothelial cell growth medium (EGM-2, Lonza, USA) containing 2% (v/v) fetal bovine serum (FBS) and 1% (v/v) penicillin-streptomycin (PS) were used at passages 4–7. Mesenchymal stem cells (MSCs) isolated from human white adipose tissue,[32] a gift from Dr. Juan M. Melero-Martin at Harvard Medical School, MA, USA, were cultured in MSC growth medium (MSCGM, Lonza, USA) containing 20% (v/v) FBS, 10 ng/mL bFGF, and 1% (v/v) PS, and used at passages 8–9. Mouse embryo NIH 3T3-L1 (BCRC, Taiwan) cultured in Dulbecco's modified Eagle's medium (DMEM, Gibco, USA) containing 10% (v/v) bovine calf serum and 1% (v/v) PS were used at passages 10–11. The medium for the co-culture of HUVECs and MSCs was 1:1 HUVEC-medium and MSC medium ratio.

Cell viability and cell behavior in hydrogels

Prepolymer solutions were gently mixed with MSCs alone (1×10^6 cells/mL) or HUVECs alone (1×10^6 cells/mL) or a mixture of MSCs (1×10^6 cells/mL) and HUVECs (1×10^6 cells/mL). After gelation under the indicated conditions, cell-laden hydrogels were formed and cultured in 24-well dishes for 2 days. After staining with a live/dead viability kit (Invitrogen, USA), the spreading area of live cells (green-labeled cells) was imaged using a multiphoton confocal microscope system (TCS-SP5-X AOBS, Leica, Germany). Serial optical sections were taken in the central depth plane concerning the surface of the hydrogel structures, and the resultant *z*-stacks were merged into an image using ImageJ to analyze the cell spreading area inside the hydrogel.

To further investigate the relationship between cell spreading and gel contraction. NIH3T3 cells were encapsulated into the α plane of the indicated hydrogel, which is vertical and horizontal to the cell culture wells, and cultured for 2 days. The macro-images were recorded on day 0 and day 2 to analyze the directions of hydrogel contraction and cell behavior. Collagen fibrils and cells were stained with Atto 425 NHS ester (Sigma Aldrich, USA), Acti-stain™ 555 phalloidin (Cytoskeleton, Inc, USA), and DAPI, and the fluorescence images were taken under confocal microscopy to investigate the directions of cell migration in the hydrogels on Day 0 and Day 2. The distance between α and β, and β and γ planes are 50 μm. Quantitative analysis was performed by calculating cell density and fibril density at α, β, and γ planes inside the hydrogels on D2 divided by that on D0 to understand the gel contraction process during cell culture.

To identify the angiogenesis-related factors secreted from mono-cultured or co-cultured cells into the hydrogel, the conditioned medium was prepared as follows. The HUVECs, MSCs, or HUVECs-MSCs cell-laden hydrogels were placed and cultured in 24-well plates in the cell growth medium supplemented with 5% FBS and allowed cells to condition the medium. After 1 day, all media were collected, centrifuged, and removed the supernatant as the conditioned medium for the following use. Angiogenesis protein array analyses of the conditioned medium were performed by proteome profiler human angiogenesis antibody array (R&D Systems, USA), which allows simultaneous analysis of 55 angiogenesis-related proteins quantitively. The preparation and incubation of the arrays were performed as recommended by the manufacturer.

To study the degrees of hypoxia and oxidative stress (ROS) on HUVECs and MSCs in hydrogels, cells were encapsulated into hydrogels and cultured in the cell culture medium supplemented with 5% FBS for 2 and 12 h. The cells were recovered by centrifugation at 100*g* for 5 min, resuspended in 0.2 mL of hypoxia/oxidative stress detection mix (2×10^5 cells/sample), and then incubated under normal culture conditions for 30 min. According to the product protocol, the hypoxia and ROS levels of cells were measured using the ROS-ID Hypoxia/Oxidative stress detection kit (Enzo Life Sciences, USA).

Measurement of volume contraction of hydrogel and tissue construct

Cell-laden collagen and collagen-Ph prepolymer were loaded into a polydimethylsiloxane (PDMS) coated glass slide, formed a disk-shaped gel, and then moved to the cell culture well to ensure the gel was non-adherent on the bottom of the well. Progression of gel contraction was captured at specific time points using a digital camera with top-view and side-view to study the area and thickness of hydrogel at each time point. The imaging conditions were manually adjusted to assure the quality of the acquired gel image. Each experimental condition was replicated four times, and the contraction rate was calculated with the area and thickness of the hydrogel on day 0. On day 7 after implantation, the implants were removed from the mice, and a three-dimensional (3D) laser scanning confocal microscope (VK-X1000, KEYENCE) was used to 3D reconstruct the volume and topography of the constructs before tissue processing for histology.

In vivo vasculogenic assay

All animal experiments were approved by the institutional animal care and use committee of National Tsing-Hua University, Taiwan (Protocol number: 108030). Five- to seven-week-old male BALB/cAnN.Cg-Foxnlnu/CrlNarl mice were purchased from the National Laboratory Animal Center, Taiwan. The formation of vascular networks in vivo was evaluated using a xenograft model through subcutaneous injection and transplantation in immunodeficient mice. For the subcutaneous injection method, the 0.2 mL prepolymer solutions were mixed with MSCs and HUVECs (3:2 ratio; 1×10^7 cells/mL) and then injected subcutaneously using 25G needles in the backs of the mice before gelation. For the transplantation method, the prepolymer solutions were mixed with MSCs and HUVECs (3:2 ratio; 1×10^7 cells/mL) before gelation. 0.2 mL of the mixture was pipetted onto a polydimethylsiloxane (PDMS)-coated glass slide, with aliquots separated by a 2 mm spacer to in vitro form a cell-laden hydrogel under the indicated crosslinking conditions. The cell-laden hydrogel constructs were then surgically implanted into subcutaneous spaces with the PDMS spacer in the backs of the mice. Each experimental condition was replicated five to seven times.

Immunofluorescence staining

Cell-laden hydrogels were fixed in 4% paraformaldehyde overnight, and the section slices were deparaffinized. Then, samples were blocked with 5% bovine serum albumin (BSA) (Sigma-Aldrich, USA) in DPBS for 30 min and incubated with anti-caspase-3 (1:100 dilution; Cell signaling Technology, USA), anti-αSMA (1:100 dilution; Abcam, USA), anti-human CD31 (1:100 dilution; Clone JC70A, Dako Cytomation, USA) antibodies, anti-mouse Ly6G antibodies (1:50 dilution; Clone1A8, eBioscience, USA), anti-mouse F4/80 antibodies (1:50 dilution; Clone CI A3-1, BD Pharmingen, USA), anti-mouse CD45 antibodies (1:50 dilution; Clone 30-F11, BD Pharmingen, USA), anti-human VEGF antibodies (1:100 dilution; R&D SYSTEM, USA), anti-MMP-9 (1:100 dilution; Abcam, USA), anti-IL-8 (1:100 dilution; Invitrogen, USA), anti-human nuclear (1:100 dilution; Clone 235-1, Abcam, UK), or anti-hypoxia-inducible factor 1 alpha (anti-HIF-1α) (1:100 dilution; Genetex, USA) at 4°C. After washing in DPBS three times,

the cell-laden hydrogels were incubated with Alexa Fluor 488-conjugated goat anti-mouse, anti-rabbit secondary antibodies, donkey anti-goat secondary antibodies (1:100 dilution; Invitrogen), Fluor 647-conjugated goat anti-rabbit or anti-mouse secondary antibodies (1:100 dilution; Invitrogen, USA) at room temperature for 1 h. Finally, they were stained with Hoechst solution (Invitrogen), immersed in DPBS, and examined using a confocal microscope (TCS-SP5-X AOBS, Leica, Germany). The cell spreading area was obtained by averaging 20 images for each of four to five samples in 200X for each condition using ImageJ software. The cell density of macrophages ($F4/80^+/CD45^+$), neutrophils ($Ly6G^+/CD^+$), and others ($CD45^+$) on tissue slices were calculated for five images of four to five samples and normalized with the volume of explants by using ImageJ software. The intensity of expression of VEGF, IL-8, or MMP-9 on tissue slices was calculated for five images of four to five samples and normalized with the volume of explants by ImageJ software.

Histological and immunohistochemical analysis staining

Tissue constructs were fixed in 4% paraformaldehyde overnight, dehydrated in ethanol, embedded in parafilm, and sectioned into 5–7 μm-thick slices. Hematoxylin and eosin (H&E) staining were used to detect lumen structures containing erythrocytes. For mouse anti-human CD31 immunohistochemical analysis, the sections were deparaffinized, and antigen retrieval was conducted by heating the sections for 30 min at 92°C in 10 mM citric acid and 0.02% Tween-20 (pH 6.0). The sections were blocked for 30 min at room temperature and incubated with mouse anti-human CD31 antibodies (1:100 dilution; Clone JC70A, Dako Cytomation, USA) at 4°C overnight. The sections were then incubated for 1 h at room temperature with HRP-conjugated secondary antibodies (1:100 dilution in blocking buffer; Vector Laboratories). The bound antibody was detected using an ImmPACT DAB substrate kit (peroxidase; Vector Laboratories, USA). Finally, the sample was counterstained with hematoxylin and mounted.

Detection and measurement of hydrogen peroxide inside tissue constructs

Previously published articles used the 3,3′-diaminobenzidine (DAB) method to detect the presence of hydrogen peroxide in plant samples.[33,34] Here, we want to detect the presence of residual H_2O_2 in implanted hydrogels in vivo, but the residual H_2O_2 might lose or become another peroxide compound after the paraffin-embedded process. To confirm whether the peroxide detected by the DAB method can represent the amount of residual H_2O_2 in collagen-based hydrogels, we added various concentrations of H_2O_2 (0–78 mM) into collagen pre-polymers. After gelation, collagen hydrogels were fixed, paraffin-embedded, cut, and deparaffinized. The sections were incubated for 1 h with 1.09 unit/mL HRP. After three times washing, the slides were detected using an ImmPACT DAB substrate kit (Vector Laboratories, USA). Finally, the sample was mounted. The quantification was analyzed by integrating total DAB intensity minus the DAB-positive nuclei regions on each slide by ImageJ software. The result (Supplemental Figure S5) showed that DAB intensities increased with concentrations of H_2O_2 solutions added into collagen hydrogels. It demonstrated that peroxide detected by DAB staining on paraffin sections-slides of collagen-based hydrogels is positively correlated to the amount of H_2O_2 added in the collagen-based hydrogel before the paraffin embedding process. Thus, DAB staining can indirectly demonstrate the presence of hydrogen peroxide.

Computational simulation

The distribution of 70 kDa dextran and oxygen in a Collagen-Ph hydrogel with or without the spacer was simulated using the diluted transport module in COMSOL Multiphysics 5.5. We simulated gel disks with a diameter of 10 mm and a thickness of 2 mm. The boundary concentrations of dextran and oxygen were set at 2 mg/mL and 0.99 g/mL, respectively. The simulation for each sample ended when dextran and oxygen were uniformly distributed in the hydrogel. The diffusion coefficients for dextran in Collagen-Ph hydrogels in the w/o and w/ spacer groups or explants were performed as follows. Briefly, the hydrogels or explants were incubated with FITC-labeled 70 kDa dextran solutions (2 mg/mL), and a time series of images was taken using fluorescence microscopy to acquire the changes in concentration as the function of time and position in hydrogels. We determined the diffusion coefficient of dextran from the image sequences by solving the diffusion equation for spatial and temporal intensity changes under non-steady conditions and a constant surface concentration. We calculated the diffusion coefficient of oxygen in our hydrogel according to the equation published literature.[35]

Statistical analysis

Three independent experiments were performed for each experimental group, with three to five replicates per experiment. The results are presented as the mean ± standard deviation. Statistical analysis was performed using one-way and two-way analysis of variance (ANOVA). Statistical significance was assumed at p-values <0.05, 0.01, and 0.001 are indicated as *, **, and ***, respectively. Pearson coefficients of correlation (r) among various parameters were analyzed and classified as following: High correlation: $|r| > 0.70$; medium correlation: $0.40 < |r| < 0.69$; low correlation: $|r| < 0.39$.

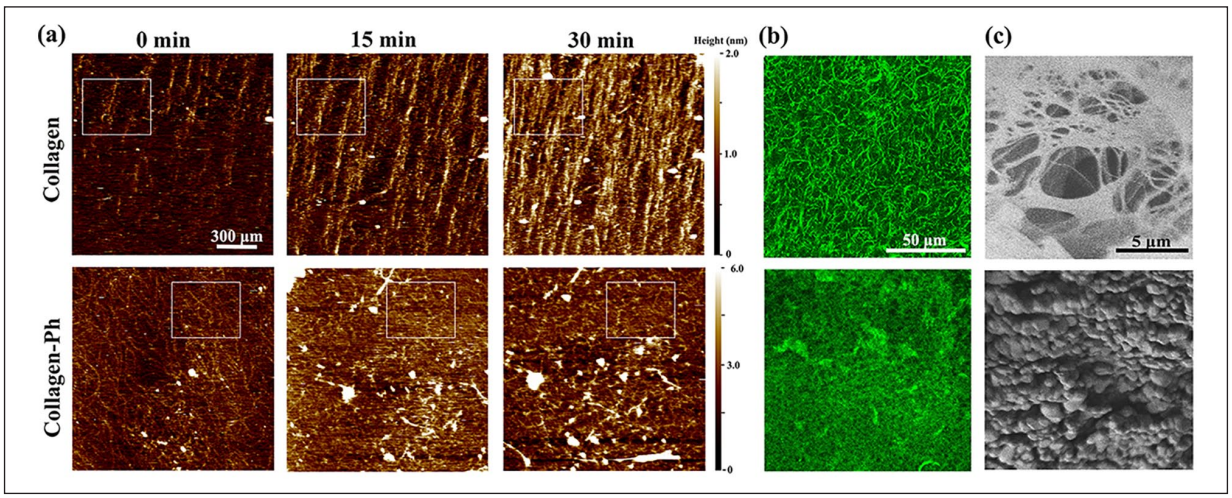

Figure 1. Kinetics of the fibril formation process and resultant microstructures of the collagen and collagen-Ph hydrogel. (a) The sequences of topography images obtained by the tapping mode of AFM, showing fibril formation of collagen and collagen-Ph prepolymers within 30 min. Scan area: $1.5 \times 1.5\ \mu m^2$. During the gelation process, collagen molecules self-assembled into a fibril (white square) along one direction to increase the length and thickness and form a fibrillar network. Collagen-Ph molecules were multi-directionally crosslinked with nearby molecules to form a honeycomb-like network (white square). Comparison of microstructures of collagen and collagen-Ph hydrogels: (b) confocal images and (c) SEM images.

Results

Fibril formation process and resulting materials properties

The collagen concentration, environmental temperature, and pH value during gelation are the primary parameters controlling the physical material properties of collagen hydrogels. Collagen molecules can self-assemble into triple helix-based fibrils to form physically-crosslinked hydrogels under conditions of concentration 0.15%–0.3%, temperature 27°C–43°C, and pH 5–8 (Supplemental Figure S1(a)–(c)). The results showed that gelation time (74–236 s), fiber diameter (0.5–1.1 μm) and length (15–22 μm), and mechanical properties (stiffness (G′): 12–138 Pa) of the collagen hydrogel could be tailored to yield a wide range of hydrogels based only on the collagen concentration. Notably, environmental temperature and pH values during gelation did not result in significant changes in these physical properties of hydrogels (Supplemental Figure S1(d)–(f)). The G′ of collagen hydrogels is highly dependent on the concentration of collagen (Supplemental Figure S1(f)). The advantage of horseradish peroxidase (HRP)-catalyzed chemical crosslinking of collagen-Ph hydrogels was the tunable G′ according to the concentration of H_2O_2, independently of the collagen concentration (Supplemental Figure S2).[7,16] To engineer vascular networks in chemical crosslinking and decouple the effects of the numbers and types of crosslinked bonds into collagen-based hydrogels from the storage modulus, collagen and collagen-Ph hydrogels with a G′ of 50 Pa were selected for the following analyses.

To investigate the formation of collagen fibrils during the gelation process, the collagen and collagen-Ph prepolymer solutions were applied to the mica substrate. Time-lapse images were captured through atomic force microscopy, providing real-time insight into collagen fibrils at the nanoscale. While the collagen solution was applied to the mica substrate at 37°C, collagen molecules started attaching to the mica surface and assembled long fibrils and transversely thicken the fibers, thereby forming a collagen hydrogel with a fibrous microstructure (upper row in Figure 1(a)). After 30 min, self-assembled collagen fibrils almost fully covered the mica surface with an oriented alignment. The formation of collagen fibrils in collagen-Ph prepolymers is multi-directional, forming a honeycomb-like microstructure during gelation (bottom row in Figure 1(a)). The confocal images showed a homogeneous finer fiber network in collagen hydrogels and a honeycomb-like structure in collagen-Ph hydrogels (Figure 1(b)). To confirm the microstructure of hydrogels, freeze-dried hydrogels were observed through scanning electron microscopy (SEM). The analysis revealed a long, thick, and interconnected fiber network in collagen hydrogels, as well as numerous small protrusions on the surface of collagen-Ph hydrogels (Figure 1(c)).

Cell-mediated contraction of hydrogels after co-culture in vitro

Numerous studies have shown that volume shrinkage in collagen hydrogels is caused by cell spreading, contraction, and movement inside a gel.[36–38] The development of chemical crosslinking methods to form covalent bonds between

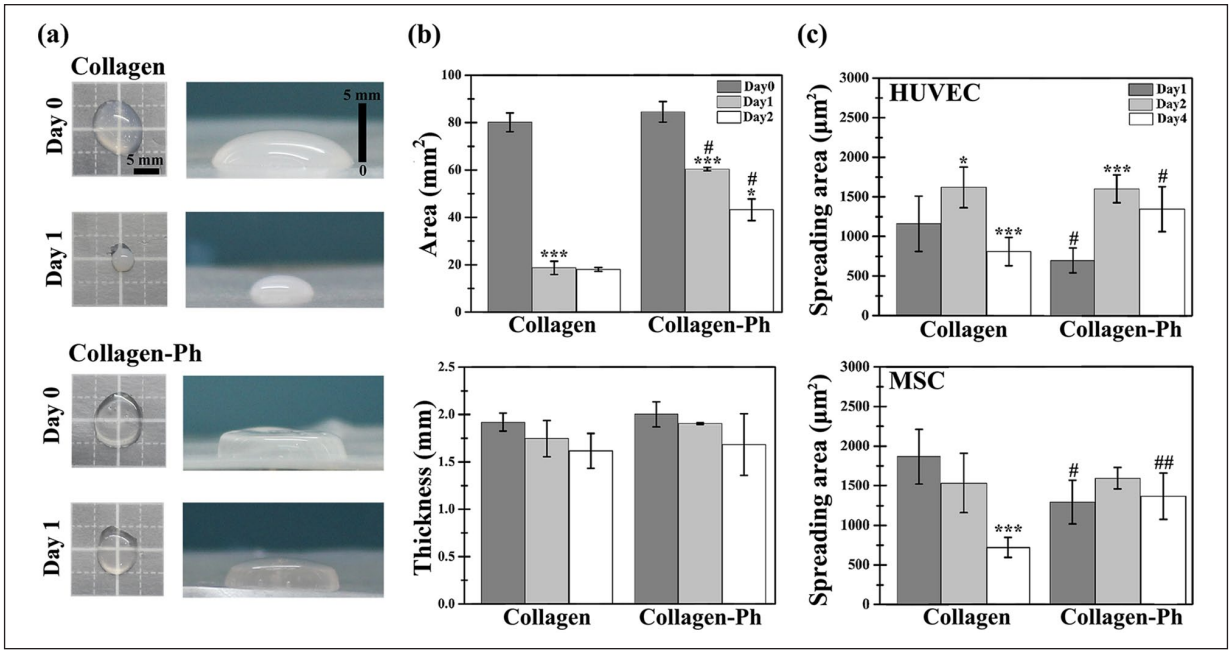

Figure 2. Cell-mediated contraction of the cell-laden collagen-based hydrogel. (a) Representative optical macroscopic images of the top view (left column) and side view (right column) of cell-laden collagen and collagen-Ph hydrogels at days 0 and 1 after culture. (b) Quantitative analysis of hydrogel contraction by measuring the area and thickness of the indicated hydrogel during culturing. (c) Spreading area of embedded HUVECs and MSCs (μm^2/cell) co-cultured into the indicated hydrogel group. Data are presented as the mean ± SD. *$p < 0.05$, ***$p < 0.001$ indicate significant differences from the prior time point in the same hydrogel group ($n = 4$–5). #$p < 0.05$ and ##$p < 0.01$ indicate significant differences from the collagen group at the same time point ($n = 4$).

collagen molecules has successfully reduced the cell-mediated volume shrinkage of hydrogels.[39–41] However, this approach has also inevitably reduced the capabilities of these hydrogels for vascular tissue engineering. In this study, macro-images were captured using a camera to record changes in the area and thickness of the hydrogel during cell culture (Figure 2(a)). The area of the cell-laden collagen hydrogel significantly decreased to ~25% on day 1 (***$p < 0.001$) and remained constant until day 2. The area of cell-laden collagen-Ph hydrogels only reduced to 60% on day 1 (***$p < 0.001$) and was further reduced to 40% on day 2 compared with day 0 (Figure 2(b)). The thickness of both cell-laden collagen and collagen-Ph hydrogels from day 0 to day 2 was similar (Figure 2(b)). Less hydrogel contraction was observed in the cell-laden collagen-Ph hydrogel compared with that noted in the collagen hydrogels, particularly in the area instead of the thickness. To clarify the relationship between hydrogel contraction and cell spreading, we investigated the cell spreading area inside both hydrogels. In collagen hydrogels, the spreading area of HUVECs was significantly increased on day 2 (*$p < 0.05$) and decreased to half on day 4 (**$p < 0.01$). The spreading area of MSCs remained constant until day 2 and was significantly decreased to a third on day 4 (***$p < 0.001$). In collagen-Ph hydrogels, the spreading area of HUVECs showed a significant two-fold increase on day 2 (***$p < 0.001$), which was maintained until day 4; notably, the spreading area of MSCs was maintained until day 4. There was no significant difference between the spreading area of HUVECs and MSCs in both types of hydrogels on day 2. Even on day 4, both cells spread well in collagen-Ph hydrogels versus collagen hydrogels. Moreover, to further understand the relationship between gel contraction and cell migration, instead of randomly encapsulating cells in the hydrogel, cells were encapsulated into the α plane of the hydrogel horizontally (Supplemental Figure S3(a)) or vertically (Supplemental Figure S3(b)) into the cell culture well. After 2 days of culture, most cells migrated to the β plane; moreover, the collagen fibril density increased along with the direction of cell migration, which may cause gel contraction in the macro scale (Supplemental Figure S3(c)–(f)). These results demonstrated that the direction of gel contraction and cell migration is opposite. In collagen-Ph hydrogels, both cells spread well, and the resulting volume remained at approximately 50% of its original volume on day 0. These findings demonstrated that collagen-Ph hydrogels attenuated the cell-mediated volume contraction under cell-spreading conditions.

Cell-laden collagen-Ph hydrogel limited the formation of vascularized soft tissue in vivo

Cell-laden prepolymers of collagen and collagen-Ph (HUVECs: MSCs, 2:3 in 10^7 cells/mL) were subcutaneously

injected into mice to determine whether the collagen-Ph hydrogel could improve the formation of vascularized soft tissues and maintain the volume of explants in vivo as well as in vitro. After 7 days, the explants were excised, and the macro-images showed a reddish color in the collagen hydrogel and white color in the collagen-Ph hydrogel, implying the presence of more blood cells within microvessels in the former versus the latter group. The resulting area of cell-laden collagen hydrogels was only a third of that of collagen-Ph hydrogels, while the thickness of both cell-laden hydrogels was approximately 0.45 mm due to compression by the skin of mice after injection (Figure 3(a) and (b)). The remaining volumes of the cell-laden collagen hydrogels and collagen-Ph hydrogels were 40% and 60% of the injected volume (~200 μL), respectively (Figure 3(b)). These results showed that cell-laden collagen-Ph hydrogels can better maintain their volume in vivo compared with collagen hydrogels.

Better biodegradability of hydrogel (i.e. the smaller remaining volume of explants) typically implies the growth of functional blood vessels in engineered soft tissue.[7] Histological and quantitative analyses of engineered blood vessels were performed to confirm whether the better remaining volume of collagen-Ph hydrogel is due to poor capability for the formation of vascular networks (Figure 3(c)–(f)). The density of perfused blood vessels (i.e. lumens with red blood cells) was eightfold higher in collagen hydrogels versus collagen-Ph hydrogels. In collagen hydrogels, microvessels were well distributed throughout the whole construct. However, in collagen-Ph hydrogels, microvessels were mainly located at the edge region of the constructs. More than 90% of perfused microvessels in both hydrogels stained positive for hCD31 and were surrounded by alpha-smooth muscle actin (αSMA)-positive pericytes. This finding demonstrated that these are engineered microvessels formed by implanted human cells. The size distribution of hCD31-positive lumens in both groups was similar, showing that engineered human microvessels are perfused, mature, and anastomosed with host vasculatures. Taken together, for unknown reasons collagen-Ph hydrogels limited the vasculogenesis of HUVECs and MSCs and anastomosis from host vasculatures. This resulted in a low density of engineered blood vessels at the subcutaneous site, which is by previous evidence.[7,16]

Increase of human VEGF expression in cell-laden collagen-Ph hydrogel

We also investigated the causes of the inability of collagen-Ph hydrogels for HUVEC- and MSC-mediated vascular soft tissue formation in vivo. For this purpose, we examined whether the capability of HUVECs and MSCs for cell-mediated vascular networks formation was impeded in collagen-Ph hydrogels during the crosslinking process and after culture compared with that noted in the collagen hydrogel. Results demonstrated that there was no difference in the percentage of viability and apoptosis of HUVECs and MSCs encapsulated into collagen and collagen-based hydrogels after culture (Supplemental Figure S4(a)–(d)). To assess the oxidative status of embedded cells in response to the gelation process, we investigated changes in the levels of hypoxia and reactive oxygen species (ROS) in HUVECs and MSCs in hydrogels after 2 and 12 h of culture in vitro (Figure 4(a)). The degree of hypoxia was similar in both groups after 2 h; nevertheless, after 12 h. it was significantly lower (0.5-fold reduction) in the collagen-Ph hydrogels versus the collagen hydrogels. ROS levels were similar in both groups after 2 h; however, after 12 h, they were significantly increased in the collagen-Ph hydrogels versus the collagen hydrogels (10-fold increase). Briefly, after 12 h of co-culture in vitro, the level of hypoxia in embedded cells decreased with increased ROS production by embedded cells in collagen-Ph hydrogels. In contrast, cells in collagen hydrogels exhibited more hypoxia and less ROS production. To further examine the effects of both hydrogels on cell paracrine signaling in embedded cells after 24 h of culture, multiple secreted angiogenic factors were examined by co-culture with conditioned medium using human angiogenesis protein arrays (Supplemental Figure S4(e) and (f) and Figure 4(b)). Secreted proangiogenic factors included VEGF, placental growth factor 2 (PlGF2), hepatocyte growth factor (HGF), several members of the insulin-like growth factor-binding protein (IGFBP) family as well as MMP-3 and -9, monocyte chemoattractant protein-1 (MCP-1), interleukin-8 (IL-8), and urokinase-type plasminogen activator (uPA). The expression of the anti-angiogenic factor, thrombospondin-1 (TSP-1) was similar. Notably, the expression of proangiogenic factors VEGF, uPA, and IL-8 was higher in collagen-Ph hydrogels versus collagen hydrogels, whereas that of MCP-1 and PIGF was lower. MSCs and HUVECs are mainly responsible for the secretion of VEGF and IL-8, respectively (Supplemental Figure S4(f) and Figure 4(b)). Several studies[42–44] showed that VEGF improves angiogenesis, while IL-8 leads to the influx of inflammatory neutrophils to deliver angiogenic MMP-9, thereby accelerating anastomosis from the host vasculature. To investigate whether the expression of VEGF, IL-8, and MMP-9 was also present in cell-laden explants on day 2 after subcutaneous injection, sectional slides were stained for histological analyses. The results showed significantly increased expression of VEGF in cell-laden collagen-Ph hydrogels versus collagen hydrogels, while the expression levels of IL-8 and MMP-9 were similar (Figure 4(c)). Increased expression of VEGF secreted by MSCs suggested improvement of angiogenesis and vasculogenesis in Collagen-Ph hydrogels. Nevertheless, the capability of collagen-Ph hydrogels to support vasculogenesis and angiogenesis in vivo remains limited. In vitro cultures may not sufficiently replicate the physiochemical conditions of vascular tissue

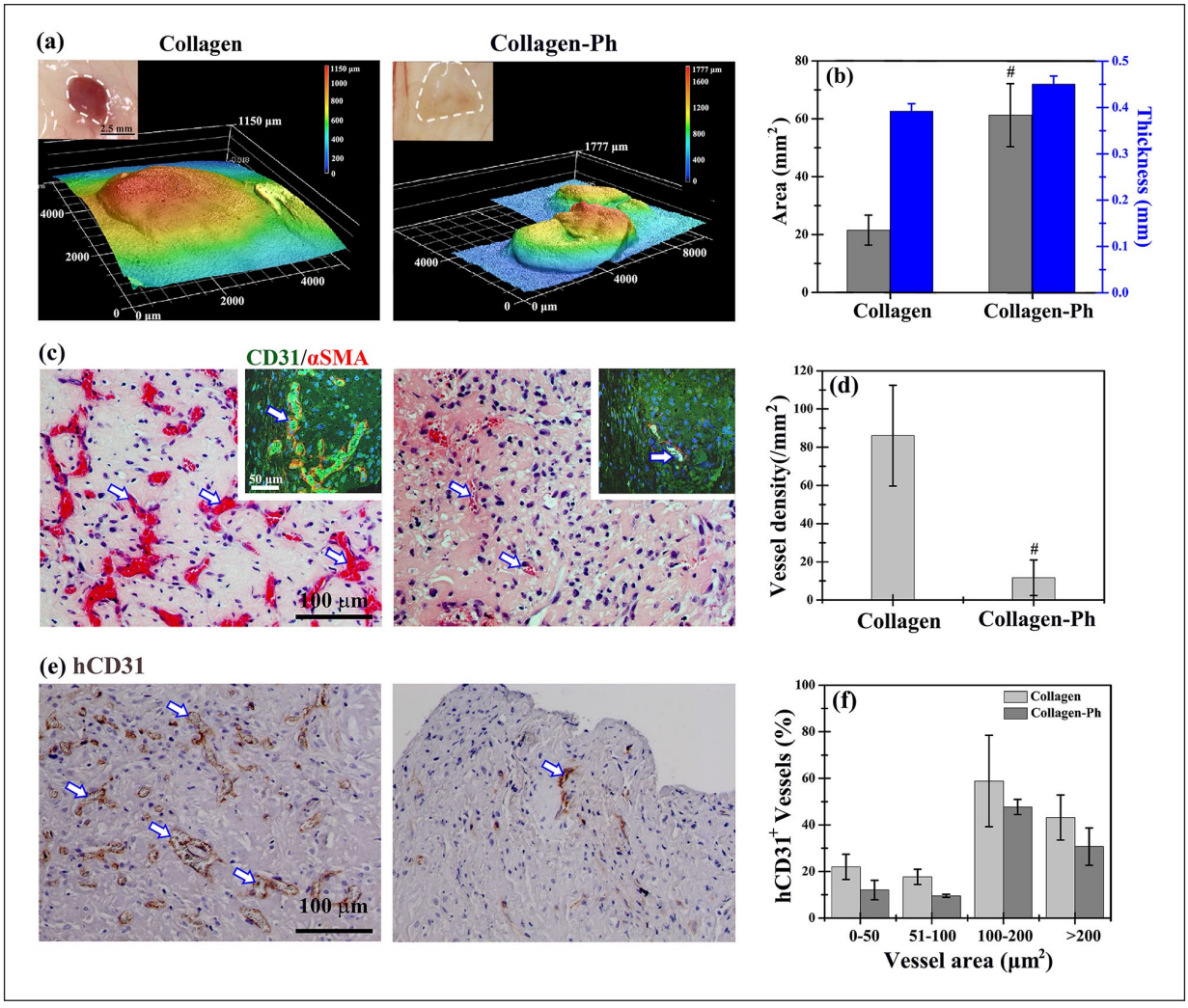

Figure 3. Hydrogel-mediated vascularized soft tissue constructs were formed at a subcutaneous site on day 7 after implantation. (a) Optical macroscopic images of the tissue construct at the subcutaneous site (inset), 3D topography images, and (b) quantitative analysis of average area and thickness of entire constructs were obtained by 3D laser scanning confocal microscopy. (c) Representative cross-sectional H&E images of tissue constructs revealed the distribution of perfused blood vessels (white arrows) in the constructs (inset). Mature perfused human vessels were lined exclusively with hCD31-expressing HUVECs (green) and surrounded by αSMA-expressing MSCs (red). Nuclei (blue) were labeled with DAPI. (d) The extent of vascular network formation was quantified by counting the densities of erythrocyte-filled lumens in H&E images. (e) Representative images of sections stained with hCD31-expressing HUVECs identified by immunohistochemistry. (f) The area distribution of human microvessels was quantified by counting hCD31+ lumens, as a percentage of the total number. #$p < 0.05$ indicates significant differences from the collagen group at the same time point.

formation in vivo, and thus other factors may be involved in attenuating the capability of collagen-Ph hydrogels for cell-mediated vascular network formation in vivo.

Presence of hydrogen peroxide prolonged the host inflammatory response

The subcutaneous injection was used for the delivery of the collagen-Ph prepolymer. The enzymatic gelation process involved the use of HRP and H_2O_2 at the subcutaneous site following injection. Several studies showed that H_2O_2 served as an early recruitment trigger for innate immune cells[45,46]; hence, the presence of H_2O_2 may induce a longer-term host immune response. We sought to confirm the presence of crosslinking agent H_2O_2 in collagen-Ph hydrogels. For this purpose, DAB staining was performed in sections of cell-laden explants on day 2 after subcutaneous injection to quantitatively detect the residual amount of H_2O_2 in explants (Figure 4(d)–(f)); brown color denoted the presence of peroxide derived from residual H_2O_2. The results showed darker brown color (1–1.5 orders of magnitude) in both acellular or cell-laden collagen-Ph hydrogels versus

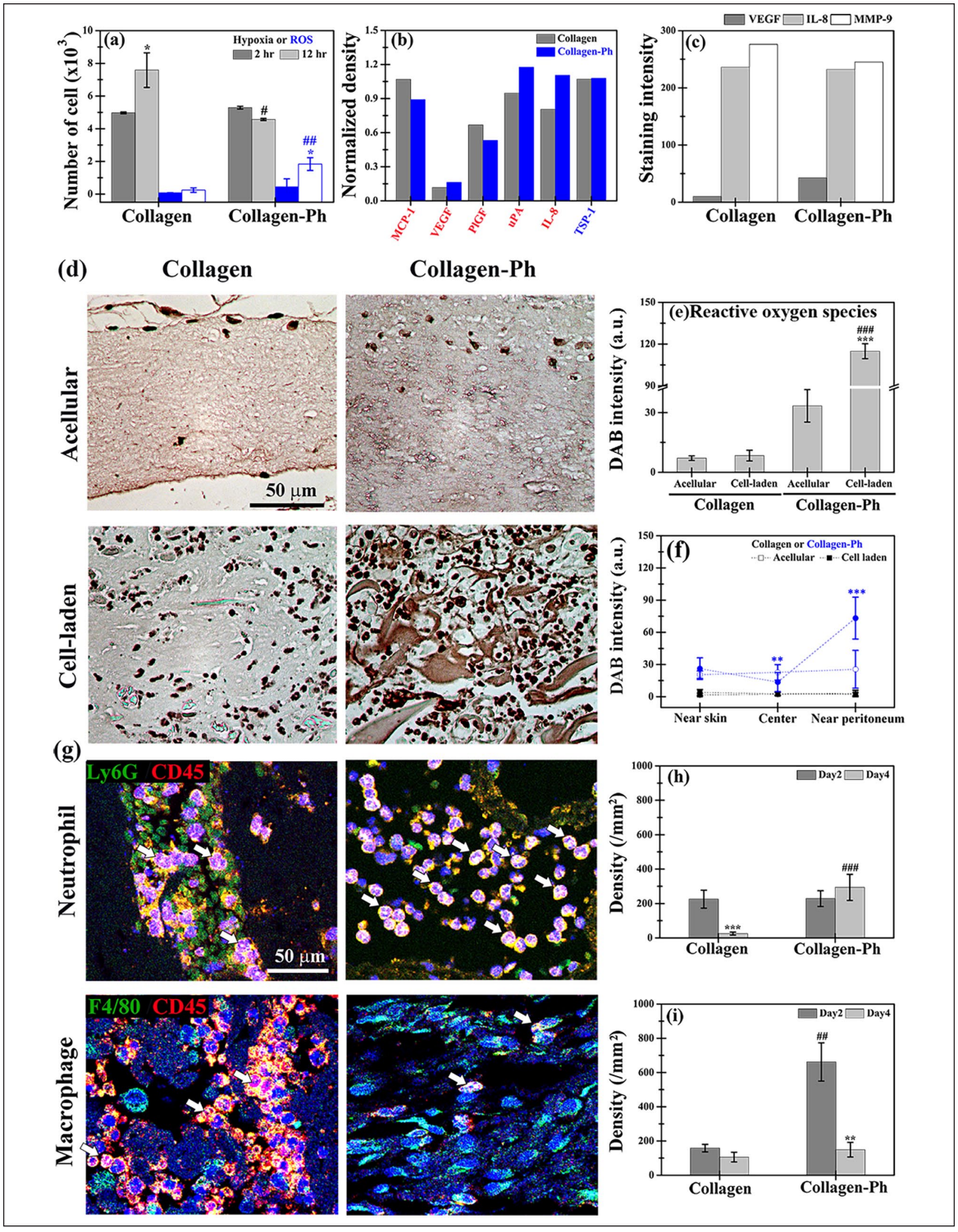

Figure 4. Longer-term host inflammatory responses were induced by subcutaneously injecting the hydrogen peroxide-triggered collagen-Ph hydrogel. (a) Numbers of ROS- and hypoxia-positive cells inside hydrogels after 2 and 12 h of culture, as detected by indicator dyes. (b) Human cytokine array analysis of conditioned medium obtained after 1 day of co-culture of HUVECs and MSCs into the collagen and collagen-Ph hydrogels. (c) Quantitative analysis of VEGF, IL-8, and MMP-9 expression in stained sectioned slices of explants on day 2 after implantation. (d) Representative DAB expression and quantitative (e) total intensity and (f) distribution analysis in stained slices sectioned from acellular and cell-laden collagen and collagen-Ph constructs on day 2 after injection. $^{***}p < 0.001$ indicates significant differences from the acellular group ($n = 3$). $\#\#p < 0.01$ and $\#\#\#p < 0.001$ indicate significant differences from the collagen group. (g) Representative immunofluorescence staining and quantification analysis of (h) Ly6G+/CD45+ neutrophils and (i) F4/80+/CD45+ macrophages in collagen and collagen-Ph constructs after injection. $^{**}p < 0.01$ and $^{***}p < 0.001$ indicate significant differences from day 2 in the same hydrogel group ($n = 4$–5). $\#\#p < 0.01$ and $\#\#\#p < 0.001$ indicate significant differences from the collagen group at the same time point.

acellular or cell-laden collagen hydrogels. Interestingly, the peroxide in the collagen-Ph hydrogel was observed 2 days after subcutaneous injection. Moreover, implantation of HUVECs and MSCs into collagen-Ph hydrogels increased the amount of peroxide found near the peritoneum. The excess peroxide detected by DAB beyond residual H_2O_2 may be attributed to an acute immune response.[47,48] The degree and timing of neutrophil and macrophage infiltration into cell-laden hydrogels play important roles in the formation of functional blood vessels.[49,50] To investigate whether the presence of H_2O_2 stimulated host inflammatory reactions, sectional slices of cell-laden explants were doubled-stained with neutrophils (Ly6G+/CD45+) and macrophages (F4/80+/CD45+) markers 2 and 4 days after subcutaneous injection (Figure 4(g)). On day 2, the densities of neutrophils were similar in both hydrogels. However, on day 4, they were significantly decreased in cell-laden collagen hydrogels to 10% and remained constant in cell-laden collagen and collagen-Ph hydrogels, respectively (Figure 4(h)). In contrast, the densities of macrophages were higher in collagen-Ph hydrogels versus collagen hydrogels (four-fold increase) on day 2, but significantly decreased to similar values on day 4 (Figure 4(i)). Overall, the cell-laden collagen-Ph hydrogels induced longer-term host immune reactions until day 4, which may delay angiogenesis, anastomosis, and vascular network formation.[51,52]

In vitro gelation and stop process decreased the host inflammatory response

To investigate the importance of longer-term immune response on vascular network formation, we immersed cell-laden collagen-Ph hydrogels into the culture medium for 1 h after ex vitro gelation to remove the residual amount of H_2O_2 and HRP (stop group). Hydrogels that were not immersed into the culture medium after gelation served as the non-stop group. Subsequently, both cell-laden collagen-Ph hydrogels were subcutaneously implanted on the back of mice. The amount of peroxide derived from residual H_2O_2, host immune response, and capability of hydrogels for vascular formation were analyzed. After 2 days of implantation, the intensity of DAB staining was significantly decreased in the stop group compared to that in the non-stop group ($\#\#p < 0.01$, Figure 5(a) and (b)) and the injected cell-laden group (Figure 4(e), $\#\#\#p < 0.001$). These findings suggested that gelation in vitro was effective in decreasing the residual amount of H_2O_2 in collagen-Ph hydrogels. We also examined whether the host immune response decreased with the decreasing amount of H_2O_2 in the stop and non-stop groups. For this purpose, the cell-laden collagen-Ph hydrogels were excised, embedded in paraffin, sectioned, and stained with markers for neutrophils and macrophages on days 2 and 4 after implantation (Figure 5(c)–(f)). The analysis revealed that, on day 2, the densities of neutrophils in both hydrogels were similar, while on day 4 the density was significantly decreased by 20% and 75% in the non-stop and stop groups, respectively (Figure 5(d)). On day 2, the density of macrophages was two-fold higher in the stop group versus the non-stop group. On day 4, it was significantly increased (+38%) in the non-stop group. On the contrary, the macrophage density in the stop group decreased by 90% from day 2 to day 4, to levels even lower than in the non-stop group (Figure 5(f)). Ex vitro gelation combined with the stop process significantly decreased the density of infiltrating neutrophils and macrophages in collagen-Ph hydrogels versus non-stop or injection ones. These findings indicate that host immune reactions to cell-laden collagen-Ph hydrogels were significantly decreased.

Decreasing host inflammatory response was not sufficient to form vascular soft tissue

To investigate whether decreasing host immune response may increase vascular formation in engineered soft tissues, cell-laden collagen-Ph hydrogels in the non-stop and stop groups were implanted into mice for 7 days to analyze the volume of the construct and capability for vascular network formation. The results showed that the volume of explants in the stop group was 50% lower than in the non-stop group, while the average thickness was 50% lower than in non-stop ones with similar areas (Figure 6(a) and (b)). Surprisingly, perfused blood vessels in histological sectional slides were barely observed in both groups (Figure 6(c) and (d)), indicating that reduction of the host immune response did not improve vascular network formation in collagen-Ph hydrogels. Thus, the host immune response is not the single determining factor limiting the vascular network formation in collagen-Ph hydrogels.

We compared the thickness before and after injection or implantation in the subcutaneous space of mice. We found that the thickness of hydrogels was significantly reduced by compression from the skin of mice after injection and implantation during daily movement of the animals. This has not been previously observed in cell culture conditions or discussed in the literature. A two-fold increase in the thickness of hydrogels resulted in a two-fold reduction in nutrient and gas transport.[53] The PDMS spacer (diameter: 10 mm; thickness: 2 mm) was designed to attenuate the compression from the mice's body skin and maintain the structural integrity of the hydrogel. Several uniform holes (diameter: 1 mm) were well distributed on the skin-side of the spacer to allow mass transport and ingrowth of host vasculature into the explant inside the spacer. To investigate whether a designed spacer could maintain the tissue volume and improve vascular formation, cell-laden collagen-Ph hydrogels in the non-stop and stop groups inside a spacer were co-implanted into mice for 7 days (Figure 7). The volume of explants in both groups (non-stop: $33.8 \pm 6\,mm^3$; stop: $30.6 \pm 2\,mm^3$; Figure 7(a) and (b))

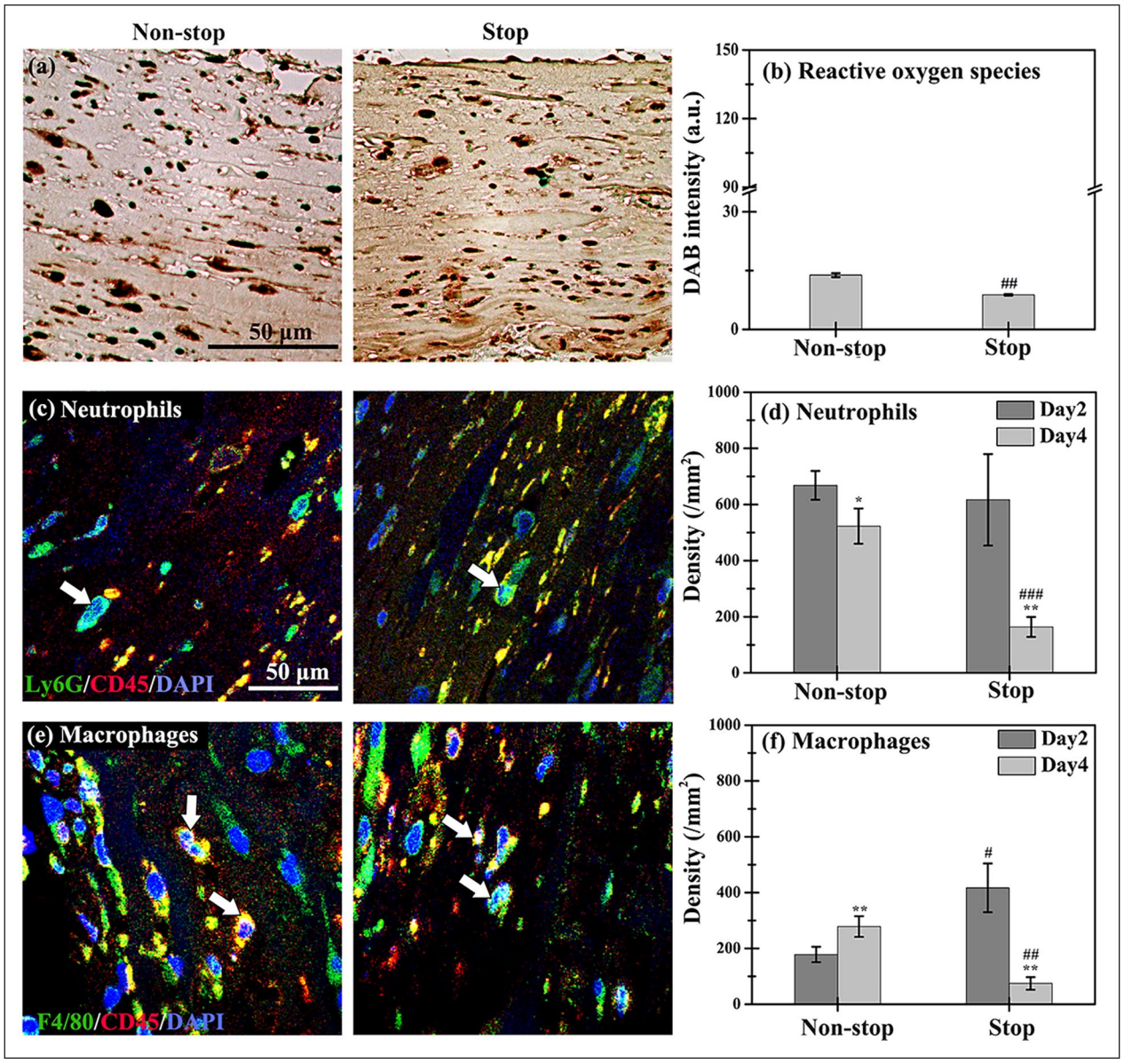

Figure 5. Through the stop process in the cell-laden collagen-Ph groups, the densities of infiltrating neutrophils and macrophages induced by the host immune response were significantly reduced on days 2–4 after implantation. (a) Representative DAB expression and (b) quantitative DAB intensity analysis in the non-stop and stop groups from the cell-laden collagen-Ph constructs removed from animals on day 2. Representative immunofluorescence staining for the densities of (c) Ly6G+ (green)/CD45+ (red) neutrophils and (e) F4/80+ (green)/CD45+ (red) macrophages. Nuclei (blue) were labeled with DAPI. Quantification of (d) Ly6G+/CD45+ neutrophils and (f) F4/80+/CD45+ macrophages on days 2 and 4 after implantation. *$p < 0.05$ and **$p < 0.01$ indicate significant differences from the prior time point in the same group. #$p < 0.05$, ##$p < 0.01$, and ###$p < 0.001$ indicate significant differences from the non-stop group at the same time point.

with the spacer was two-fold greater than that measured in those without the spacer (Figure 6(a) and (b)) by maintaining the thickness and area of explants. Notably, there was a three-fold greater number of perfused blood vessels in the histological slides of explants in the stop groups (52.9 ± 1.6 #/mm^2) versus the non-stop group (10.6 ± 7 #/mm^2) (Figure 7(c) and (d)). These results demonstrated that volume support and reduction of the host immune response can significantly improve vascular network formation in collagen-Ph hydrogels. More than 90% of perfused microvessels in both hydrogels were stained positive for hCD31 and surrounded by αSMA-positive pericytes, demonstrating that they are engineered human microvessels. The size distribution of hCD31-positivelumens in the stop group with spacer support was greater than that recorded in the non-stop group.

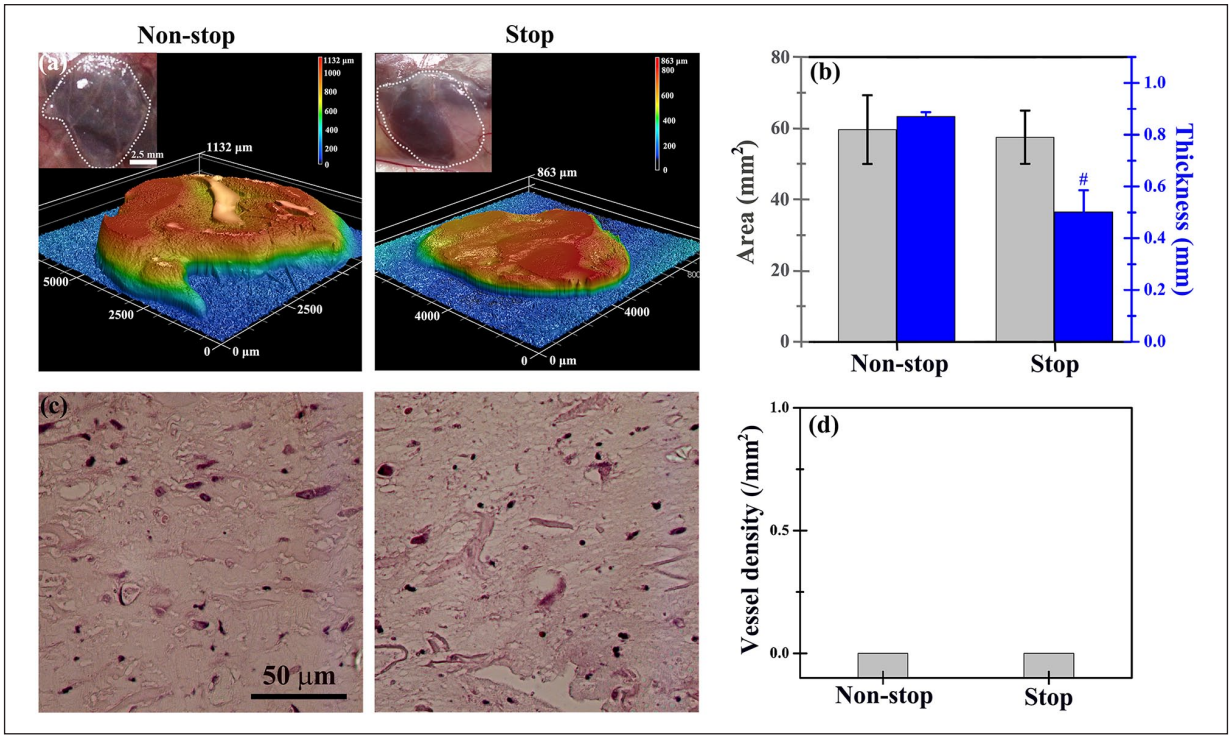

Figure 6. In the absence of a spacer, cell-laden collagen-Ph structures in the stop or non-stop group did not maintain the volume of the engineered constructs and did not support the formation of vascular networks on day 7 after implantation. (a) Optical macroscopic images of a tissue construct at a subcutaneous site (inset), 3D topography images, and (b) quantitative analysis of the entire explant volume (i.e. area and thickness) were performed by 3D laser scanning confocal microscopy. (c) Representative cross-sectional H&E images of the tissue constructs did not reveal lumens or perfused blood vessels in the structures. (d) Vessel density in the engineered tissue constructs was removed 7 days after implantation. #$p < 0.05$ indicates significant differences from the non-stop group.

Effects of the designed spacer on cells embedded in collagen-Ph hydrogels

We investigated the effects of the designed spacer on mass transport in cell-laden collagen-Ph hydrogels in vivo. Before implantation, there was no difference in diffusion properties of both collagen and collagen-Ph hydrogels (Supplemental Figures S6(a)). Collagen-Ph hydrogels with and without spacer were subcutaneously implanted and excised to study the diffusion properties of hydrogels at 4, 8, 12, and 24 h after surgery (Supplemental Figures S6(b)). After immersing the explants in dextran solutions to measure the depth of diffusion over time, the diffusion coefficient in the with-spacer group (1.6×10^{-6} cm^2/s) was 10-fold higher than that recorded in the without-spacer group (7.4×10^{-7} cm^2/s). The results showed that the spacer improved the diffusivity of the hydrogel by maintaining the structural integrity of hydrogels to avoid compression from the skin. Due to an inadequate oxygen supply to tissues and cells, new vessels with red blood cells form in vivo in response to hypoxia,[54,55] which induces angiogenesis. Thus, the oxygen concentration is generally an indicator of the capability for vascular network formation. After performing calculations as previously described,[35] the diffusivity of oxygen in both groups was found to be similar (without-spacer group: 2.13×10^{-5} cm^2/s; with-spacer group: 2.17×10^{-5} cm^2/s). To further investigate the oxygen distribution inside hydrogels, a computational simulation based on the three-dimensional finite element method was conducted. For the calculation of diffusion coefficients and the thickness of explants, the concentration profiles of dextran (Figure 8(a) and (b)) and oxygen (Figure 8(c) and (d)) were plotted against location and time in both groups according to the diffusion equation. In the without-spacer group, the final concentration of dextran in the hydrogel was maximized, and its distribution within the gel was uniform (dark red regions in the left panel of Figure 8(a) and (c)). In the with-spacer group, there was a 2.4- and 4-fold increase versus the without-spacer group in the time required to reach a uniform distribution of dextran and oxygen concentration, respectively. The addition of a designed spacer caused hypoxia in some regions of the hydrogel (yellow to blue regions in the right panel of Figure 8(a) and (c)), which may induce local hypoxia in embedded cells. Hypoxia through HIF-1α leads to angiogenesis involving VEGF signaling during the regeneration process.[56,57] VEGF staining was performed on explants 2 and 4 days after implantation to investigate whether the observed low concentration

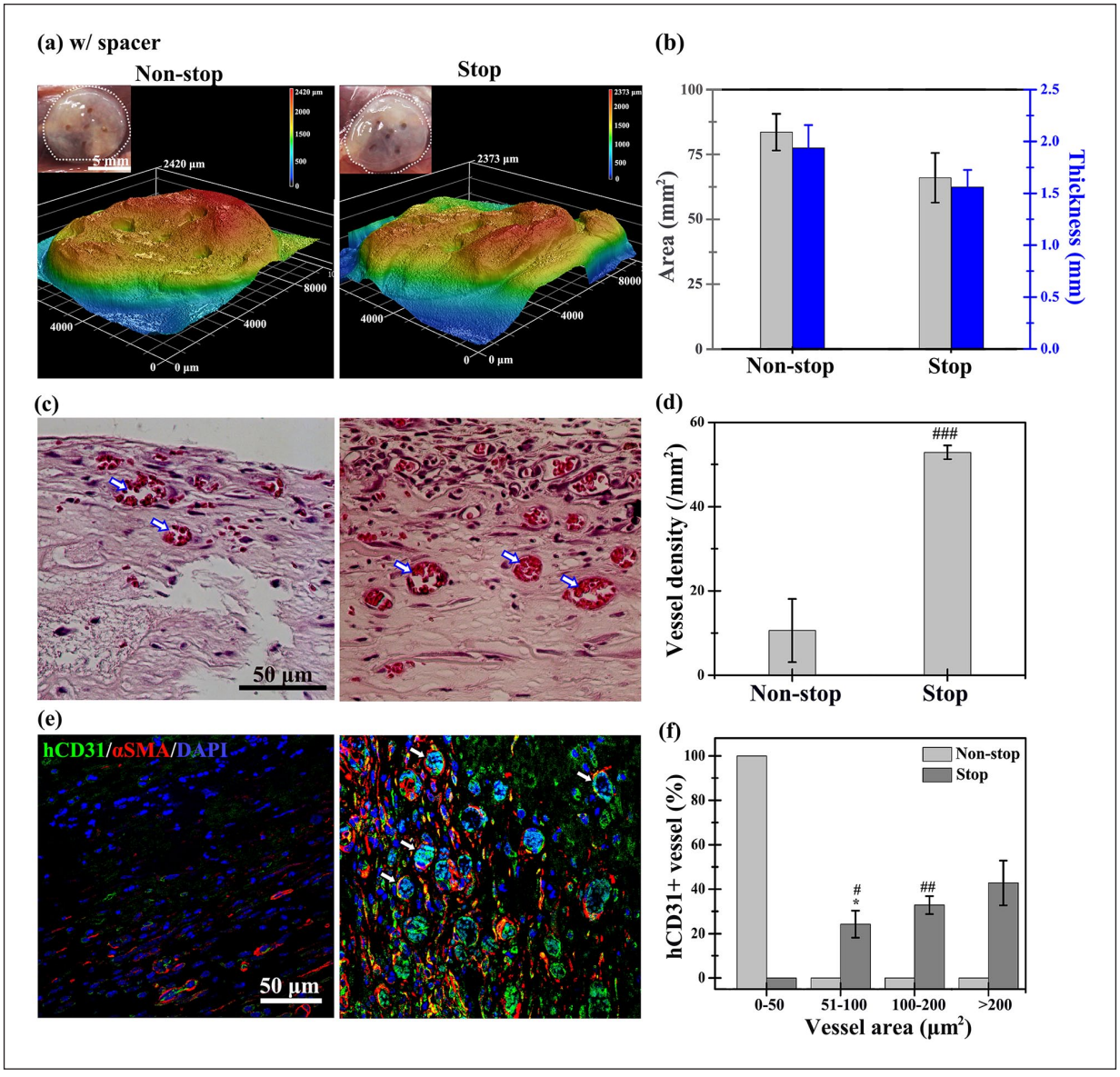

Figure 7. Using a spacer, cell-laden collagen-Ph structures in the stop group maintained the volume of the engineered constructs and supported the formation of vascular networks on day 7 after implantation. (a) Optical macroscopic images of the tissue construct at a subcutaneous site (inset), and (b) quantitative analysis of the entire construct volume (i.e. area and thickness) were obtained by 3D laser scanning confocal microscopy. (c) Representative cross-sectional H&E images of the tissue constructs revealed perfused blood vessels (labeled with white arrows) in the structures. (d) The extent of vascular network formation was quantified by counting the densities of erythrocyte-filled lumens. (e) Representative images of mature perfused human vessels were lined exclusively with hCD31-expressing HUVECs (green) and surrounded by αSMA-expressing MSCs (red). Nuclei (blue) are labeled with DAPI. (f) Area of hCD31+ human microvessels, as a percentage of the total area. *$p < 0.05$ indicates significant differences from the vessel area with 0–50 μm^2 in the same group ($n = 3$). #$p < 0.05$, ##$p < 0.01$, and ###$p < 0.001$ indicate significant differences from the non-stop group.

of oxygen induces hypoxia in embedded cells, thereby improving vascular network formation (Figure 8(e) and (f)). The results of the quantitative analysis showed that the expression of HIF-1α and VEGF in the with-spacer group was 1.5- and 2-fold higher than that measured in the without-spacer group on day 2 after implantation, respectively. It has been shown that hypoxia induces VEGF secretion in embedded HUVECs and MSCs.[58,59] Thus, the increase in human-specific VEGF implied that the level of hypoxia in cells was increased by adding the designed spacer. This effect may improve microvessel formation in oxygen-sufficient cell-laden collagen-Ph hydrogels.

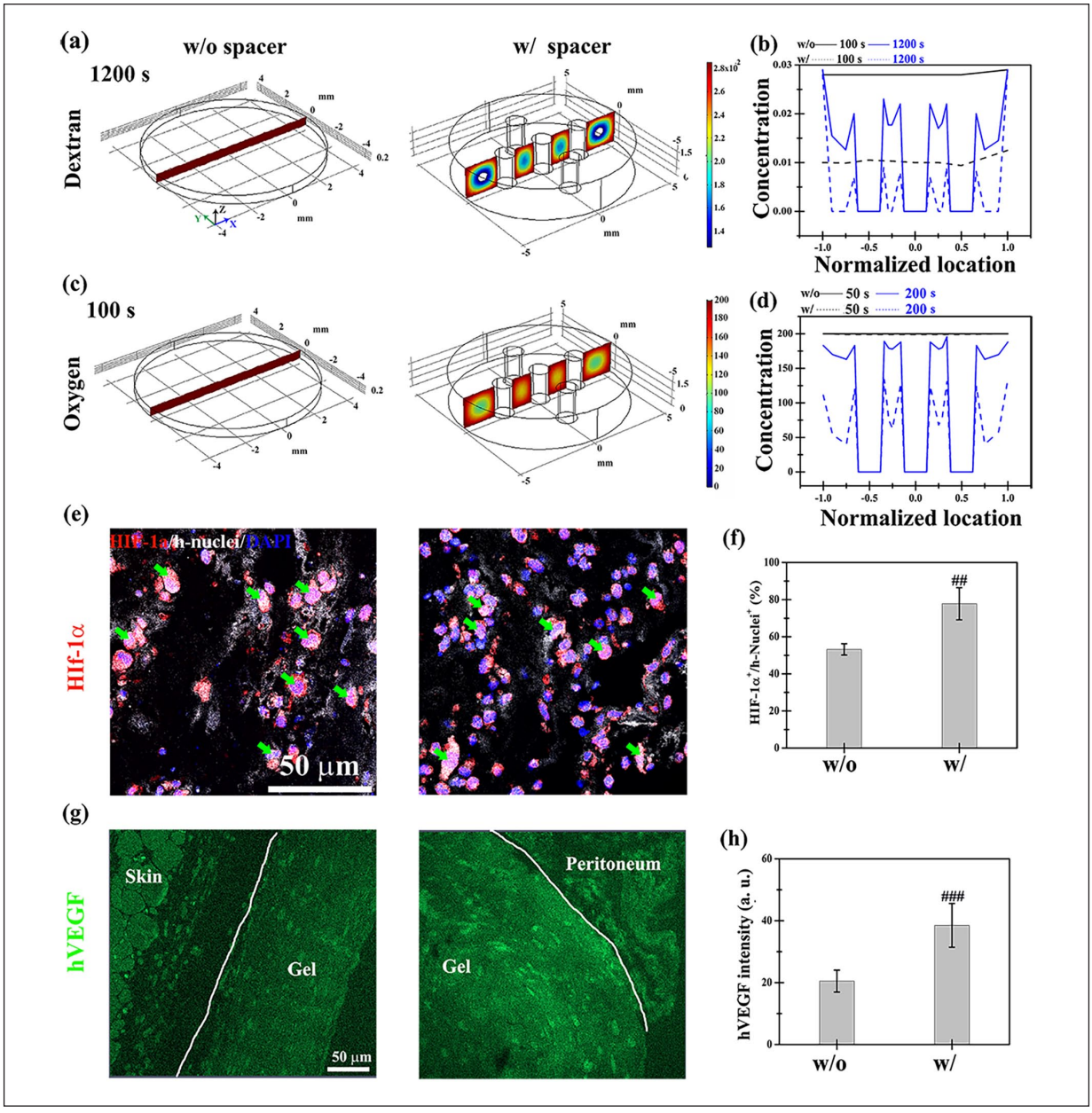

Figure 8. Transport properties of nutrients and oxygen in the cell-laden hydrogel with and without the support of a designed spacer at the subcutaneous site of mice. Dextran (molecular weight: 70 kDa) served as a transport tracer for nutrients. Three-dimensional computational simulation of (a) dextran and (c) oxygen transport properties in cell-laden hydrogels at the indicated time points. The distribution of (b) dextran and (d) oxygen at the center plane of the construct at different time points. Representative fluorescence images and quantitative analysis of the expression of (e and f) HIF-1α and human nuclei (h-nuclei) and (g and h) human-specific VEGF in the with- and without-spacer groups in the collagen-Ph constructs removed from animals on day 2. ##$p < 0.01$ and ###$p < 0.001$ indicate significant differences from the w/ spacer group.

Discussion

The longer-term immune response is a key factor limiting vascular network formation in cell-laden collagen-Ph hydrogels

Several groups pointed out some concerns on the high concentration and long retention time of natural and chemical cross-linking agents in chemical-crosslinked hydrogels during and after gelation process,[60,61] which significantly reduced the cell viability and function in cell-culture or animals.[62–64] But, few studies investigated how it affects tissue regeneration in vivo. Here, the concentration of crosslinking agents (H_2O_2), delivery method, diffusion efficiency, and resulting immune response of chemically crosslinked hydrogels were discussed to improve the capability of

microvessels formation in hydrogen peroxide triggered chemical crosslinked collagen-Ph hydrogel. More ROS production in embedded HUVECs and MSCs were observed in collagen-Ph hydrogels compared to those in the collagen hydrogel (Figure 4(a)), which cause fewer cells in hypoxia states in the collagen-Ph hydrogel due to more oxygen production in the enzymatic catalyzed chemical reaction of HRP and H_2O_2 during gelation process[65,66] of the Collagen-Ph hydrogel. A basal level of ROS is necessary for basic biological processes of cells, including cellular proliferation and differentiation. It was published that production of ROS at a low concentration of H_2O_2 (0.1–10 μM) stimulate angiogenesis through increased secretion of angiogenesis factors VEGF and FGF-2 in MSCs,[67] while the high concentration (>125 μM) of H_2O_2 causes cell damage.[68] The 28.5 μM of H_2O_2 used in this study to crosslink collagen-Ph hydrogels was proved non-cytotoxic to cell viability and spreading of HUVECs and MSCs in vitro.[16] To further investigate whether the presence of H_2O_2 affected the capability of vascular network formation of HUVECs and MCSs during the chemically crosslinking process, we pretreated both cells with 28.5 μM of H_2O_2 for 30 min and then encapsulated them into physically crosslinking Collagen hydrogels to evaluate the capabilities of vascular network formation compared with non-treated ones (the Collagen group) (Supplemental Figures S7). Of note, in realistic conditions, the concentration of H_2O_2 was consumed and decreased during crosslinking process of collagen-Ph hydrogel, and it is hard to in situ measure the concentration changes during gelation, so we used 28.5 μM of H_2O_2 applied at the beginning to do this test, which is the harshest condition to the treated cells. In the H_2O_2 treated groups, microvessels densities remained constant, but the coverage rate of MSCs on HUVECs decreased significantly to 20% (Supplemental Figures S7). These results demonstrated that excess ROS production induced by H_2O_2 in MSCs decreased the capability of MSCs to serve as pericytes to support and stabilize vascular network formation in vivo. Some studies showed ROS stimulates the induction of VEGF expression in various cell types through HIF-1α-VEGF signaling.[69–71] Here, higher expression of VEGF was observed in the cell-laden collagen-Ph hydrogels (Supplemental Figure S8) implied that appropriated concentration of H_2O_2 can stimulate secretion of VEGF in MSCs through increasing ROS to stimulate angiogenesis, which are accordance with our observation in cells culture (Figure 4(b) and (c)). However, it still cannot explain why there were only limited microvessels formed into the border region of cell-laden collagen-Ph implants at the subcutaneous site in the presence of a high concentration of VEGF (Figures 3(c)–(f), 4(b) and (c)).

Several studies demonstrated that the concentrations of H_2O_2 are proportional to numbers of infiltrating immune cells, showing H_2O_2 is the mediator for host immune response.[72,73] These results were by our observation that longer-term immune responses and the presence of H_2O_2 coexisted into the cell-laden collagen-Ph hydrogel after 2 days of injection. To decrease the remaining amount of H_2O_2, we prepared cell-laden collagen-Ph hydrogels in vitro, and after 30 min of gelation, it was immersed into the medium to wash out excess H_2O_2 (Figure 5(a) and (b)) before implantation. To confirm the negative effect from excess H_2O_2, collagen-Ph hydrogels in the Stop group were immersed into the H_2O_2 solutions for 2 h, and then co-implanted with spacer into the subcutaneous site of mice. On day 2 and day 4, the numbers of neutrophils and macrophages in the Sop group with the addition of H_2O_2 are significantly higher than in the Stop group. After 7 days, no blood vessels were observed in collagen-Ph hydrogels (Supplemental Figures S9 and S10(a)). The addition of hydrogen peroxide into the Stop group caused a stronger and longer immune response, which inhibited vascular network formation. On the contrary, the immune response in the Stop group significantly decreased on day 4 after implantation, which confirmed the longer-term host immune response observed into collagen-Ph hydrogels was contributed by the residual H_2O_2 and following induced host immune cells. Even though the immune response was successfully attenuated by immersing into culture medium before implantation (the stop + w/o spacer group), densities of engineered microvessels inside collagen-Ph hydrogels were dropped to near 0 after 7 days, which is significantly lower than that in the injection group (non-stop conditions, $p < 0.001$, Figure 3(c)–(e), Supplemental Figure S10(a)). These demonstrated the longer-term immune response is one of the factors to limit vascular network formation in cell-laden collagen-Ph hydrogels.

Coexisting sufficient VEGF and attenuated immune response support vascular network formation in cell-laden in cell-laden collagen-Ph hydrogels

According to our observations in experimental animals, hydrogels were compressed by the skin after injection and implantation. We therefore designed and co-implanted a spacer with cell-laden hydrogels to maintain the structural integrity of hydrogels at the subcutaneous site and avoid compression from the skin of mice. Computer simulations of oxygen and dextran transport into cell-laden hydrogels with and without support from a spacer were conducted to investigate the effects of the designed spacer on microvessel formation (Figure 8). Following the addition of the spacer, the diffusivity of hydrogels increased by one order and the thickness of explants showed a five-fold increase. These effects decreased the concentration of oxygen and nutrients in the central region of collagen-Ph hydrogels. This led to a greater number of hypoxic cells in this oxygen- and nutrient-deficient region. The highest VEGF expression and prolonged

host immune response were observed in the non-stop + with spacer group. These observations may be attributed to the generation of ROS during gelation and spacer-induced hypoxia. Moreover, vascular network formation was increased to ~10 ± 7 #/mm^2 (Supplemental Figure S10(b)). The non-stop + without-spacer and injection groups as well as the stop + with-spacer group showed similar VEGF expression (~40 a.u.; Supplemental Figure S10(b)), probably due to ROS-stimulated and hypoxia-induced secretion of VEGF in MSCs, respectively. Interestingly, in these three groups with similar VEGF expression, the densities of engineered microvessels were inversely proportional to the immune response (Supplemental Figure S10(a); Pearson coefficient $r = -0.95$). In the non-stop + with-spacer group, the content of VEGF was the highest among the groups (~72 a.u.; Supplemental Figure S10(b)). Nevertheless, the resulting lumen density followed the inversely proportional relationship between the immune response and lumen density observed in the non-stop + without-spacer, injection, and the stop + with-spacer groups (Supplemental Figure S10(a)). The Pearson coefficient for the non-stop + without-spacer, non-stop + with-spacer, injection, and stop + with-spacer groups was $r = -0.94$, implying that the immune response was dominant in the presence of a sufficient amount of VEGF in the explants. A higher amount of VEGF did not contribute to the extra increase in the number of microvessels. In contrast, the lowest VEGF expression (~20 a.u.) and immune response (~−82%) were observed in the stop + without-spacer group, which did not exhibit microvessel formation (~0 #/mm^2). This may be due to the insufficient amount of VEGF. To confirm the importance of VEGF, exogenous VEGF (100 ng/mL) was added into the stop + without-spacer group during gelation. Seven days after implantation, the results showed that the densities of microvessels formed into collagen-Ph hydrogels were significantly increased from 0 to ~19 #/mm^2 (Supplemental Figure S11). Incorporation of this result into the correlation analysis between immune response and microvessel density revealed that the engineered lumen density in engineered tissues is inversely proportional to the immunological response to cell-laden implants (Supplemental Figure S12, $r = -0.78$, high correlation). Here, we provided a strategy to improve cell-mediated vascular network formation in the hydrogen peroxide-triggered collagen-Ph hydrogel by using the designed spacer to induce hypoxia to encapsulated cells, but this may need a second surgery to remove this non-biodegradable silicone spacer after repair in the clinical setting. To address this concern, a biodegradable and biocompatible 10% GelMA–20% polyethylene glycol dimethacrylate (PEGDMA 1000)[74,75] spacer was prepared by casting and light irradiation (Supplemental Figure S13). Thus, the material composition of the spacer can be tailored and altered according to the intended biomedical applications. Taken together, for engineering cell-mediated vascular networks in collagen-Ph hydrogels, it is necessary to simultaneously have sufficient VEGF and attenuated host immune response to cell-laden collagen-Ph hydrogels for the first 4 days after implantation.

Conclusion

Collagen-Ph hydrogels can successfully reduce cell-mediated volume contraction, but the capability of these hydrogels for cell-mediated blood vessel network formation is limited due to long the host inflammation response induced by crosslinking reagents and the presence of ROS generated during gelation. After consuming unreacted crosslinkers (H_2O_2) and providing a designed spacer to increase hypoxia in cells embedded in hydrogels, the density of engineered blood vessels in the hydrogels was significantly increased. Our findings suggest that the duration of host immune response and sufficient levels of VEGF play important roles in the self-assembly of embedded cells in H_2O_2-triggered chemically-crosslinked collagen-Ph hydrogels at a subcutaneous site in animals. These results provide valuable information for expanding the capabilities of other enzymatic-catalyzed chemically-crosslinked hydrogels used in in vitro cell culture and in vivo vascular tissue engineering.

Authors' Note

Feng-Sheng Kao is now affiliated to Department of Microstructure and Characterization, Industrial Technology Research Institute, Hsinchu, Taiwan.

Author contributions

Shih-Yen Wei contributed to the design and characterization of materials, in vitro cell culture work, animal studies, and histological staining and data analysis. Tzu-Hsuan Chen performed SEM analysis, and the modeling and simulation studies. Feng-Sheng Kao performed AFM studies to in situ observed the gel formation process analysis. Yi-Jung Hsu conducted some animal surgeries and perfusion with Shih-Yen Wei. Ying-Chieh Chen conducted some animal surgeries, interpreted results, and wrote the manuscript. All authors discussed results and provided suggestions for the manuscript.

Declaration of conflicting interests

The author(s) declared no potential conflicts of interest with respect to the research, authorship, and/or publication of this article.

Funding

The author(s) disclosed receipt of the following financial support for the research, authorship, and/or publication of this article: This work was supported by grants from the Ministry of Science and Technology of Taiwan (MOST 107-2221-E-007-067-MY3 and MOST 109-2628-E-007-001-MY3). The authors acknowledge the core facility of the Multiphoton and Confocal Microscope System at the College of Biological Science and Technology, National Yang-Ming Chiao Tung University, Hsinchu, Taiwan for cell imaging. We would like to thank Uni-edit (www.uni-edit.net) for editing and proofreading this manuscript.

ORCID iD

Ying-Chieh Chen https://orcid.org/0000-0001-9754-5362

Supplemental material

Supplemental material for this article is available online.

References

1. Rioja AY, Tiruvannamalai Annamalai R, Paris S, et al. Endothelial sprouting and network formation in collagen- and fibrin-based modular microbeads. *Acta Biomater* 2016; 29: 33–41.
2. Lu KG and Stultz CM. Insight into the degradation of type-I collagen fibrils by MMP-8. *J Mol Biol* 2013; 425: 1815–1825.
3. Lauer-Fields JL, Juska D and Fields GB. Matrix metalloproteinases and collagen catabolism. *Biopolymers* 2002; 66: 19–32.
4. Ferreira AM, Gentile P, Chiono V, et al. Collagen for bone tissue regeneration. *Acta Biomater* 2012; 8: 3191–3200.
5. Li Y, Meng H, Liu Y, et al. Fibrin gel as an injectable biodegradable scaffold and cell carrier for tissue engineering. *Sci World J* 2015; 2015: 1–10.
6. Allen P, Melero-Martin J and Bischoff J. Type I collagen, fibrin and PuraMatrix matrices provide permissive environments for human endothelial and mesenchymal progenitor cells to form neovascular networks. *J Tissue Eng Regen Med* 2011; 5: E74–E86.
7. Chuang CH, Lin RZ, Melero-Martin JM, et al. Comparison of covalently and physically cross-linked collagen hydrogels on mediating vascular network formation for engineering adipose tissue. *Artif Cells Nanomed Biotechnol* 2018; 46: S434–S447.
8. Fitzsimmons REB, Ireland RG, Zhong A, et al. Assessment of fibrin-collagen co-gels for generating microvessels ex vivo using endothelial cell-lined microfluidics and multipotent stromal cell (MSC)-induced capillary morphogenesis. *Biomed Mater* 2021; 16: 035005.
9. Nien YD, Han YP, Tawil B, et al. Fibrinogen inhibits fibroblast-mediated contraction of collagen. *Wound Repair Regen* 2003; 11: 380–385.
10. Davidenko N, Campbell JJ, Thian ES, et al. Collagen-hyaluronic acid scaffolds for adipose tissue engineering. *Acta Biomater* 2010; 6: 3957–3968.
11. Orban JM, Wilson LB, Kofroth JA, et al. Crosslinking of collagen gels by transglutaminase. *J Biomed Mater Res Part A* 2004; 68: 756–762.
12. Wang L and Stegemann JP. Glyoxal crosslinking of cell-seeded chitosan/collagen hydrogels for bone regeneration. *Acta Biomater* 2011; 7: 2410–2417.
13. Tirella A, Liberto T and Ahluwalia A. Riboflavin and collagen: new crosslinking methods to tailor the stiffness of hydrogels. *Mater Lett* 2012; 74: 58–61.
14. Amri MA, Firdaus MA, Fauzi MB, et al. Cytotoxic evaluation of biomechanically improved crosslinked ovine collagen on human dermal fibroblasts. *Biomed Mater Eng* 2014; 24: 1715–1724.
15. Lai J-Y. Biocompatibility of chemically cross-linked gelatin hydrogels for ophthalmic use. *J Mater Sci Mater Med* 2010; 21: 1899–1911.
16. Kuo KC, Lin RZ, Tien HW, et al. Bioengineering vascularized tissue constructs using an injectable cell-laden enzymatically crosslinked collagen hydrogel derived from dermal extracellular matrix. *Acta Biomater* 2015; 27: 151–166.
17. Lee F, Chung JE and Kurisawa M. An injectable hyaluronic acid-tyramine hydrogel system for protein delivery. *J Control Release* 2009; 134: 186–193.
18. Xu K, Lee F, Gao SJ, et al. Injectable hyaluronic acid-tyramine hydrogels incorporating interferon-α2a for liver cancer therapy. *J Control Release* 2013; 166: 203–210.
19. Ziadlou R, Rotman S, Teuschl A, et al. Optimization of hyaluronic acid-tyramine/silk-fibroin composite hydrogels for cartilage tissue engineering and delivery of anti-inflammatory and anabolic drugs. *Mater Sci Eng C* 2021; 120: 111701.
20. Jin R, Teixeira LS, Dijkstra PJ, et al. Enzymatically-crosslinked injectable hydrogels based on biomimetic dextran-hyaluronic acid conjugates for cartilage tissue engineering. *Biomaterials* 2010; 31: 3103–3113.
21. Xu K, Narayanan K, Lee F, et al. Enzyme-mediated hyaluronic acid-tyramine hydrogels for the propagation of human embryonic stem cells in 3D. *Acta Biomater* 2015; 24: 159–171.
22. Kumar P, Ciftci S, Barthes J, et al. A composite gelatin/hyaluronic acid hydrogel as an ECM mimic for developing mesenchymal stem cell-derived epithelial tissue patches. *J Tissue Eng Regen Med* 2020; 14: 45–57.
23. Lee F, Chung JE and Kurisawa M. An injectable enzymatically crosslinked hyaluronic acid–tyramine hydrogel system with independent tuning of mechanical strength and gelation rate. *Soft Matter* 2008; 4: 880–887.
24. Wang L, Li J, Zhang D, et al. Dual-enzymatically crosslinked and injectable hyaluronic acid hydrogels for potential application in tissue engineering. *RSC Adv* 2020; 10: 2870–2876.
25. Zhang Y, Chen H, Zhang T, et al. Injectable hydrogels from enzyme-catalyzed crosslinking as BMSCs-laden scaffold for bone repair and regeneration. *Mater Sci Eng C Mater Biol Appl* 2019; 96: 841–849.
26. Sakai S, Hirose K, Taguchi K, et al. An injectable, in situ enzymatically gellable, gelatin derivative for drug delivery and tissue engineering. *Biomaterials* 2009; 30: 3371–3377.
27. Park KM, Ko KS, Joung YK, et al. In situ cross-linkable gelatin–poly(ethylene glycol)–tyramine hydrogel via enzyme-mediated reaction for tissue regenerative medicine. *J Mater Chem* 2011; 21: 13180–13187.
28. Wang LS, Du C, Chung JE, et al. Enzymatically cross-linked gelatin-phenol hydrogels with a broader stiffness range for osteogenic differentiation of human mesenchymal stem cells. *Acta Biomater* 2012; 8: 1826–1837.
29. Hong S, Kim JS, Jung B, et al. Coaxial bioprinting of cell-laden vascular constructs using a gelatin-tyramine bioink. *Biomater Sci* 2019; 7: 4578–4587.
30. Park KM, Lee Y, Son JY, et al. In situ SVVYGLR peptide conjugation into injectable gelatin-poly(ethylene glycol)-tyramine hydrogel via enzyme-mediated reaction for enhancement of endothelial cell activity and neo-vascularization. *Bioconjug Chem* 2012; 23: 2042–2050.
31. Chuang CH, Lin RZ, Tien HW, et al. Enzymatic regulation of functional vascular networks using gelatin hydrogels. *Acta Biomater* 2015; 19: 85–99.

32. Chen YC, Lin RZ, Qi H, et al. Functional human vascular network generated in photocrosslinkable gelatin methacrylate hydrogels. *Adv Funct Mater* 2012; 22: 2027–2039.
33. Daudi A and O'Brien JA. Detection of hydrogen peroxide by DAB staining in *Arabidopsis* leaves. *Bio Protoc* 2012; 2 (18): e263.
34. Kuźniak E, Świercz U, Chojak J, et al. Automated image analysis for quantification of histochemical detection of reactive oxygen species and necrotic infection symptoms in plant leaves. *J Plant Interact* 2014; 9: 167–174.
35. Lee SY, Lee BR, Lee J, et al. Microscale diffusion measurements and simulation of a scaffold with a permeable strut. *Int J Mol Sci* 2013; 14: 20157–20170.
36. Gentleman E, Nauman EA, Dee KC, et al. Short collagen fibers provide control of contraction and permeability in fibroblast-seeded collagen gels. *Tissue Eng* 2004; 10: 421–427.
37. Liu XD, Skold M, Umino T, et al. Endothelial cell-mediated type I collagen gel contraction is regulated by hemin. *J Lab Clin Med* 2000; 136: 100–109.
38. Zhu YK, Umino T, Liu XD, et al. Contraction of fibroblast-containing collagen gels: initial collagen concentration regulates the degree of contraction and cell survival. *In Vitro Cell Dev Biol Anim* 2001; 37: 10–16.
39. Yang K, Sun J, Guo Z, et al. Methacrylamide-modified collagen hydrogel with improved anti-actin-mediated matrix contraction behavior. *J Mater Chem B* 2018; 6: 7543–7555.
40. Lotz C, Schmid FF, Oechsle E, et al. Cross-linked collagen hydrogel matrix resisting contraction to facilitate full-thickness skin equivalents. *ACS Appl Mater Interfaces* 2017; 9: 20417–20425.
41. Lee JC, Pereira CT, Ren X, et al. Optimizing collagen scaffolds for bone engineering: Effects of cross-linking and mineral content on structural contraction and osteogenesis. *J Craniofac Surg* 2015; 26: 1992–1996.
42. Li B, Wang H, Zhou G, et al. VEGF-loaded biomimetic scaffolds: a promising approach to improve angiogenesis and osteogenesis in an ischemic environment. *RSC Adv* 2017; 7: 4253–4259. Article.
43. Guo D, Murdoch CE, Xu H, et al. Vascular endothelial growth factor signaling requires glycine to promote angiogenesis. *Sci Rep* 2017; 7: 14749.
44. Zhang ZG, Zhang L, Jiang Q, et al. VEGF enhances angiogenesis and promotes blood-brain barrier leakage in the ischemic brain. *J Clin Investig* 2000; 106: 829–838.
45. Yoo SK and Huttenlocher A. Innate immunity: wounds burst H_2O_2 signals to leukocytes. *Curr Biol* 2009; 19: R553–R555.
46. Kohchi C, Inagawa H, Nishizawa T, et al. ROS and innate immunity. *Anticancer Res* 2009; 29: 817–821.
47. Kobayashi SD, Malachowa N and DeLeo FR. Neutrophils and bacterial immune evasion. *J Innate Immun* 2018; 10: 432–441.
48. Erttmann SF and Gekara NO. Hydrogen peroxide release by bacteria suppresses inflammasome-dependent innate immunity. *Nat Commun* 2019; 10: 3493.
49. Lin R-Z, Lee CN, Moreno-Luna R, et al. Host non-inflammatory neutrophils mediate the engraftment of bioengineered vascular networks. *Nat Biomed Eng* 2017; 1: 0081.
50. Lin RZ, Chen YC, Moreno-Luna R, et al. Transdermal regulation of vascular network bioengineering using a photopolymerizable methacrylated gelatin hydrogel. *Biomaterials* 2013; 34: 6785–6796.
51. Winter RL, Tian Y, Caldwell FJ, et al. Cell engraftment, vascularization, and inflammation after treatment of equine distal limb wounds with endothelial colony forming cells encapsulated within hydrogel microspheres. *BMC Vet Res* 2020; 16: 43.
52. Sun G, Zhang X, Shen YI, et al. Dextran hydrogel scaffolds enhance angiogenic responses and promote complete skin regeneration during burn wound healing. *Proc Natl Acad Sci USA* 2011; 108: 20976–20981.
53. McMurtrey RJ. Analytic models of oxygen and nutrient diffusion, metabolism dynamics, and architecture optimization in three-dimensional tissue constructs with applications and insights in cerebral organoids. *Tissue Eng Part C Methods* 2016; 22: 221–249.
54. Chen L, Endler A and Shibasaki F. Hypoxia and angiogenesis: regulation of hypoxia-inducible factors via novel binding factors. *Exp Mol Med* 2009; 41: 849–857.
55. Yamakawa M, Liu LX, Date T, et al. Hypoxia-inducible factor-1 mediates activation of cultured vascular endothelial cells by inducing multiple angiogenic factors. *Circ Res* 2003; 93: 664–673.
56. Zimna A and Kurpisz M. Hypoxia-inducible factor-1 in physiological and pathophysiological angiogenesis: applications and therapies. *Biomed Res Int* 2015; 2015: 549412.
57. Oladipupo S, Hu S, Kovalski J, et al. VEGF is essential for hypoxia-inducible factor-mediated neovascularization but dispensable for endothelial sprouting. *Proc Natl Acad Sci USA* 2011; 108: 13264–13269.
58. Liu J, Hao H, Xia L, et al. Hypoxia pretreatment of bone marrow mesenchymal stem cells facilitates angiogenesis by improving the function of endothelial cells in diabetic rats with lower ischemia. *PLoS One* 2015; 10: e0126715.
59. Liu YX, Cox SR, Morita T, et al. Hypoxia regulates vascular endothelial growth factor gene expression in endothelial cells: identification of a 5′-enhancer. *Circ Res* 1995; 77: 638–643.
60. Abu-Hakmeh A, Kung A, Mintz BR, et al. Sequential gelation of tyramine-substituted hyaluronic acid hydrogels enhances mechanical integrity and cell viability. *Med Biol Eng Comput* 2016; 54: 1893–1902.
61. Wu ZM, Zhang XG, Zheng C, et al. Disulfide-crosslinked chitosan hydrogel for cell viability and controlled protein release. *Eur J Pharm Sci* 2009; 37: 198–206.
62. Poursamar SA, Lehner AN, Azami M, et al. The effects of crosslinkers on physical, mechanical, and cytotoxic properties of gelatin sponge prepared via in situ gas foaming method as a tissue engineering scaffold. *Mater Sci Eng C Mater Biol Appl* 2016; 63: 1–9.
63. Fessel G, Cadby J, Wunderli S, et al. Dose- and time-dependent effects of genipin crosslinking on cell viability and tissue mechanics – toward clinical application for tendon repair. *Acta Biomater* 2014; 10: 1897–1906.
64. Moriarty N, Pandit A and Dowd E. Encapsulation of primary dopaminergic neurons in a GDNF-loaded collagen hydrogel increases their survival, re-innervation and function after intra-striatal transplantation. *Sci Rep* 2017; 7: 16033.

65. Wang R, Li J, Chen W, et al. A biomimetic mussel-inspired ε-poly-l-lysine hydrogel with robust tissue-anchor and anti-infection capacity. *Adv Funct Mater* 2017; 27: 1604894.
66. Wakabayashi R, Ramadhan W, Moriyama K, et al. Poly(ethylene glycol)-based biofunctional hydrogels mediated by peroxidase-catalyzed cross-linking reactions. *Polym J* 2020; 52: 899–911.
67. Huang YJ and Nan GX. Oxidative stress-induced angiogenesis. *J Clin Neurosci* 2019; 63: 13–16.
68. Kim YW and Byzova TV. Oxidative stress in angiogenesis and vascular disease. *Blood* 2014; 123: 625–631.
69. Zhou Y, Yan H, Guo M, et al. Reactive oxygen species in vascular formation and development. *Oxid Med Cell Longev* 2013; 2013: 1–14.
70. Xia C, Meng Q, Liu L-Z, et al. Reactive oxygen species regulate angiogenesis and tumor growth through vascular endothelial growth factor. *Cancer Res* 2007; 67: 10823–10830.
71. Zhu H and Zhang S. Hypoxia inducible factor-1α/vascular endothelial growth factor signaling activation correlates with response to radiotherapy and its inhibition reduces hypoxia-induced angiogenesis in lung cancer. *J Cell Biochem* 2018; 119: 7707–7718.
72. Wittmann C, Chockley P, Singh SK, et al. Hydrogen peroxide in inflammation: messenger, guide, and assassin. *Adv Hematol* 2012; 2012: 541471.
73. Niethammer P, Grabher C, Look AT, et al. A tissue-scale gradient of hydrogen peroxide mediates rapid wound detection in zebrafish. *Nature* 2009; 459: 996–999.
74. Hutson CB, Nichol JW, Aubin H, et al. Synthesis and characterization of tunable poly(ethylene glycol): gelatin methacrylate composite hydrogels. *Tissue Eng Part A* 2011; 17: 1713–1723.
75. Bertassoni LE, Cecconi M, Manoharan V, et al. Hydrogel bioprinted microchannel networks for vascularization of tissue engineering constructs. *Lab Chip* 2014; 14: 2202–2211.